

ANALYSIS OF NOVEL MTA NUCLEOSIDASE INHIBITORS
AS ANTI-PARASITIC AGENTS

by

Teslin Marie Botoy

A thesis

submitted in partial fulfillment
of the requirements for the degree of
Master of Science in Chemistry
Boise State University

August 2015

© 2015

Teslin Marie Botoy

ALL RIGHTS RESERVED

BOISE STATE UNIVERSITY GRADUATE COLLEGE

DEFENSE COMMITTEE AND FINAL READING APPROVALS

of the thesis submitted by

Teslin Marie Botoy

Thesis Title: Analysis of novel MTA nucleosidase inhibitors as anti-parasitic agents

Date of Final Oral Examination: 19 June 2015

The following individuals read and discussed the thesis submitted by student Teslin Marie Botoy, and they evaluated her presentation and response to questions during the final oral examination. They found that the student passed the final oral examination.

Kenneth A. Cornell, Ph.D.

Chair, Supervisory Committee

Eric Brown, Ph.D.

Member, Supervisory Committee

Kristen Mitchell, Ph.D.

Member, Supervisory Committee

The final reading approval of the thesis was granted by Kenneth Cornell, Ph.D., Chair of the Supervisory Committee. The thesis was approved for the Graduate College by John R. Pelton, Ph.D., Dean of the Graduate College.

DEDICATION

To my husband, Ryan, whose encouragement and love made this work possible.

ACKNOWLEDGEMENTS

I owe a great debt of gratitude to my advisor, Dr. Ken Cornell, who has pushed me to be a true scientist. I also owe thanks to Dr. Eric Brown, Dr. Shin Pu, and Dr. Kristen Mitchell for their advice and involvement on my thesis committee. Many thanks as well to Dr. Danny Xu at Idaho State University School of Pharmacy for his work and dedication to this thesis. Without him, this thesis would not have been possible. I am also grateful to Jake Schaefer, Lauren Hosek, and Ryan Carfi, for all of their work on this thesis. Lastly, I would also like to thank my fellow lab rats: Amy Hall, Jason Stonick, Reese Knippel, Ben Lew, Catherine Jambura, and Necia Hunter.

This thesis research was supported by grants from the Idaho Beef Council, the Idaho IDeA Network for Biomedical Research Excellence programs (P20RR016454, P20GM103408), the Institute for Translational Health Science (University of Washington), the M. J. Murdock Charitable Trust, and Center for Biomedical Research Excellence (COBRE P20GM109095). Without these grants, none of this would have been possible and I am forever grateful for the support.

ABSTRACT

The parasitic protozoa *Giardia intestinalis* and *Entamoeba histolytica* are major health concerns and responsible for hundreds of millions of cases of intestinal disease per year. Strains of both parasites have been discovered that show resistance to metronidazole, the most prevalent treatment for these pathogens. Thus, there is a need to identify new drugs and drug targets to combat the growing threat of drug resistant parasites. The parasite enzyme methylthioadenosine nucleosidase (MTN) is one such potential target. Traditional drug development processes take almost a decade and hundreds of millions of dollars to complete. In an effort to shorten that timeline and reduce development costs, the drugs tested in this study were found by *in silico* screening of a drug library containing thousands of small molecules to identify a subset of compounds that showed theoretical high binding affinities to the *E. coli* MTN enzyme. Enzymatic screening of the 33 tightest binding drugs yielded four potent inhibitors of *E. coli* MTN that also showed inhibitory activity against target parasite MTNs. The inhibition profiles of these drugs against parasite MTNs and the human enzyme methylthioadenosine phosphorylase (MTAP) were extensively characterized. The drugs were also tested against live cell cultures of *Giardia intestinalis* and human cell lines for growth inhibitory activity. The drug 5A (N-(2-furyl methyl)-N'-(4-nitrophenyl)urea) showed an IC₅₀ of 10.8 μM against *Giardia intestinalis* cultures, while exhibiting an IC₅₀ of over 100 μM against human cells. These results suggest that the MTN inhibitors

identified in this work are potential lead compounds for further development, and that *in silico* drug screening is an effective strategy for identifying anti-parasitic agents.

TABLE OF CONTENTS

DEDICATION	iv
ACKNOWLEDGEMENTS	v
ABSTRACT	vi
LIST OF TABLES	x
LIST OF FIGURES	xi
LIST OF ABBREVIATIONS.....	xiii
CHAPTER ONE: INTRODUCTION.....	1
Parasites	1
<i>Giardia intestinalis</i>	4
<i>Entamoeba histolytica</i>	8
Methionine, SAM Reactions, and the Methionine Salvage Pathway	10
Methylthioadenosine Nucleosidase (MTN): A New Drug Target.....	14
In-silico Computational Drug Discovery	22
Summary	26
CHAPTER TWO: MATERIALS AND METHODS	27
Induction and Purification of Recombinant Enzymes	27
Analysis of MTN and MTAP Proteins	28
Determination of Protein Concentration.....	29
MTN Activity: Enzyme Assays	29

MTN Inhibition Assay	30
Cell Growth Assays	31
<i>Giardia intestinalis</i> Resazurin Reduction Assay	31
<i>Giardia intestinalis</i> BacTiter-Glo™ Assay	32
Mammalian Cell Line Resazurin Reduction Assays	32
CHAPTER THREE: RESULTS AND DISCUSSION.....	34
Purity and Activity of Proteins	34
MTN Inhibition Assays.....	39
<i>Giardia intestinalis</i> Drug Sensitivity	44
Human Cell Line Drug Sensitivity	47
CHAPTER FOUR: CONCLUSION.....	50
REFERENCES	51
APPENDIX A.....	60
Structures and Properties of the Best MTN Inhibitors.....	60
APPENDIX B.....	62
Substrate Kinetics Graphs.....	62
APPENDIX C.....	65
Graphs of Inhibition Kinetics.....	65
APPENDIX D.....	70
Compounds Identified from In Silico Screening	70

LIST OF TABLES

Table 1.	World Wide Prevalence of Parasitic Infections	3
Table 2	Summary of Recombinant Parasite MTN Substrate Kinetics.....	38
Table 3	IUPAC Names of MTN Inhibitors.....	39
Table 4	Summary of Drug Discrimination Factors.....	44
Table 5	Summary of Drug IC ₅₀ Values (in μ M)	49
Table A.1	Structures and Properties of the Best MTN Inhibitors.....	61
Table D.1	Compounds Identified from <i>In-Silico</i> Screening	71

LIST OF FIGURES

Figure 1.	<i>Giardia intestinalis</i> Life Cycle (CDC, 2014 a).....	6
Figure 2.	<i>Entamoeba histolytica</i> Life Cycle (CDC, 2014 b).....	8
Figure 3.	SAM Synthesis.....	11
Figure 4.	The Methionine Salvage Cycle.....	12
Figure 5.	Methyltransferase Reactions.....	13
Figure 6.	Polyamine Synthesis.....	14
Figure 7.	Radical SAM Reactions.....	15
Figure 8.	Alternative Polyamine Synthesis Pathway for Putrescine.....	17
Figure 9.	Clustal W Alignment of MTN Sequences.....	18
Figure 10.	MTN vs. MTAP Active Site Electrostatic Maps.....	19
Figure 11.	MTA Transition and its Analogues.....	21
Figure 12.	<i>E. coli</i> MTN Active Site Electrostatic Maps with Bound Inhibitors.....	25
Figure 13.	SDS-PAGE of Recombinant Proteins.....	34
Figure 14.	Substrate-velocity Graph of GI MTN-1 for MTA.....	37
Figure 15.	<i>Giardia</i> MTN-1 Inhibition Kinetics for Drug 27A.....	40
Figure 16.	Summary of Ki values.....	42
Figure 17.	Resazurin reduction assay.....	45
Figure 18.	BacTiter-Glo™ reaction.....	45
Figure 19.	<i>Giardia intestinalis</i> Drug Sensitivity Graphs.....	46
Figure 20.	Human Cell Line Sensitivity to MTN Inhibitors.....	48

Figure B1.	EH MTN Substrate Kinetic Graphs	63
Figure B2.	GI MTN-1 Substrate Kinetic graphs.....	63
Figure B3.	GI MTN-2 Substrate Kinetic Graphs.....	64
Figure C1.	EH MTN Inhibition Kinetics Graphs.....	66
Figure C2.	GI MTN-1 Inhibition Kinetics Graphs	67
Figure C3.	GI MTN-2 Inhibition Kinetics Graphs	68
Figure C4.	Human MTAP Inhibition Kinetics Graphs.....	69

LIST OF ABBREVIATIONS

5'dADO	5' Deoxyadenosine
AdoMet	S-adenosylmethionine
AMP	Adenosine monophosphate
ARGd	Arginine deaminase
ATP	Adenosine triphosphate
B-PER	Bacterial protein extraction reagent
dcSAM	decarboxylated S-adenosylmethionine
DMEM	Dulbecco's Modified Eagle Medium
DNA	Deoxyribonucleic acid
DI	Deionized
EC	<i>Escherichia coli</i>
EH	<i>Entamoeba histolytica</i>
FBS	Fetal Bovine Serum
FDA	Food and Drug Administration
GI	<i>Giardia intestinalis</i>
GI MTN-1	<i>Giardia intestinalis</i> MTN enzyme encoded by 798 bp gene
GI MTN-2	<i>Giardia intestinalis</i> MTN enzyme encoded by 885 bp gene
HTS	High throughput screening
IPA	Isopropyl Alcohol
IPTG	Isopropyl β -D-1-thiogalactopyranoside

LB	Luria Bertani Broth
MAT	Methionine Adenosyltransferase
mRNA	Messenger Ribonucleic Acid
MTA	5'-Methylthioadenosine
MTAP	5'-Methylthioadenosine Phosphorylase
MTN	5'-Methylthioadenosine Nucleosidase
MTR	5-Methylthioribose
MTR-1-P	Methylthioribose-1-phosphate
OCT	Ornithine carbomyl transferase
OD	Optical Density
Odc	Ornithine decarboxylase
PBS	Phosphate Buffered Saline
PPi	Pyrophosphate
Pi	Phosphate ion
RPM	Revolutions per minute
RPMI	Roswell Park Memorial Institute 1640 medium
SAH	S-Adenosylhomocysteine
SAHH	S-Adenosylhomocysteine Hydrolase
SAM	S-Adenosylmethionine
SAMdc	SAM decarboxylase
SDS PAGE	Sodium Dodecyl Sulfate Polyacrylamide Gel Electrophoresis
SEM	Standard error on the mean
Spds	Spermidine synthase

TSA	Transition State Analog
TYDK	Tryptone Yeast Diamond Keister medium
WHO	World Health Organization

CHAPTER ONE: INTRODUCTION

Parasites

The word parasite comes from the Greek, *parasitos*, which means “beside food” and was the name used for servers at feasts. The word evolved to describe sycophants who hung around banquets for table scraps. In science, the definition has evolved to describe any organism that survives by taking nutrients from a host that suffers from the arrangement. Certain bacteria and viruses could equally fit this definition but they are classified separately for historical reasons (Zimmer, 2000).

Parasites that live inside a host (endoparasites) include protozoa (*e.g.*, *Giardia intestinalis*, *Entamoeba histolytica*), digeneans (*e.g.*, *Schistosoma mansoni*), cestodes (*e.g.*, *Taenia solium*), nematodes (*e.g.*, *Trichinella spiralis*), and acanthocephalans (*e.g.*, *Moniliformis clarkia*). Parasites that live outside the host (ectoparasites) include arthropods (*e.g.*, *Ixodes* tick) and most monogeneans (*e.g.*, *Diplozoon paradoxum*) (Bush, Fernandez, Esch, & Seed, 2001). It is thought that most parasites started out as free-living creatures that evolved in order to survive on or inside other living things. This evolution is proposed to have proceeded in a stepwise manner, where the initial requirement was parasite-host interaction that included some form of pre-adaptation to the host environment to allow full time occupancy of host tissues. It was also an evolutionary imperative that the parasites have a better chance of survival while associated with the host than they would as free-living creatures (Poulin, 2007).

Anthropologists have proposed that approximately half the humans who have ever lived, likely died from some form of parasitic infection (Drisdelle, 2010). This assertion, though impossible to prove, may be true. Parasites are the largest category of infectious diseases. They have evolved mechanisms that allow them to survive varying conditions inside and outside the host, and can be found infecting all known species of higher organisms (Roberts & Janovy, 2013).

Parasitic illnesses are often considered “diseases of poverty.” This is an oversimplification of the real impact of parasitic infection. According to the Oxford Poverty and Human Development Initiative’s Multidimensional Poverty Index, approximately 1.6 billion of the 7 billion people inhabiting the planet are living in abject poverty (Alkire & Seth, 2013). The World Health Organization considers infectious disease a large contributing factor to poverty. Lifting the burden of infectious disease would automatically improve the over-all economic future of humanity. Proof of this principle can be seen in the economic advantages resulting from the near eradication of dracunculiasis or guinea worm disease. Inexpensive water filters, community outreach, and education programs have allowed millions of people who were formerly at risk of losing months of income while afflicted with the worm to work, go to school, and otherwise improve their chances of economic stability (Cairncross, Müller, & Zagaria, 2002).

Parasite Scientific Name	Parasite Common Name	Estimated World Prevalence	Estimated Mortality Rank	Relative U.S. Prevalence
<i>Giardia intestinalis</i>	Giardiasis "beaver fever"	2-3 billion	Low	1-2 million per year
<i>Toxoplasma gondii</i>	Toxoplasmosis	1-2.5 billion	Very low	Low
<i>Trichomonas vaginalis</i>	Trichomoniasis	15% of women	Very low	Considered a common STD
<i>Entamoeba histolytica</i>	Amebiasis	200-400 million	No. 2	Low
<i>Plasmodium spp.</i>	Malaria	200-300 million	No. 1	Low
<i>Schistosoma mansoni</i>	Schistosomiasis	200-300 million	No. 3*	Uncommon
<i>Trypanosoma spp.</i>	Chagas disease "African Sleeping sickness"	15-20 million	No. 3*	Increasing in U.S.
<i>Leishmania spp.</i>	Leishmaniasis	12 million	No. 3*	Large concern of U.S. military

Adapted from Thom & When, 2012. * tie ranking due to a lack of accurate data.

The mortality and morbidity due to parasitic diseases are enormous (Table 1). Worse, parasites are incredibly difficult to kill without causing harm to their host, since they share so much in common with the host at the cellular and metabolic level. Thus, there are relatively few anti-parasitic drugs available, and most of them have some degree of toxicity to humans, particularly with repeated or prolonged use. For example, malaria, which causes the most deaths annually of any of the parasites, has approximately eight different commonly used treatments. Most of these anti-malarials have toxicities that limit their use in young children or pregnant women. Unfortunately, these are the same patient populations that are most likely to suffer severe forms of the disease and are at the highest risk of death from malaria (CDC, 2013). Despite issues of drug toxicity, a measure of pseudo-control over parasitic infections has been achieved with the help of

environmental management to reduce vector transmission, and the use of anti-parasitic agents. Unfortunately, this has resulted in selective pressures that have pushed both arthropod vectors and parasites to adapt and evolve drug resistance. Isolates of drug resistant parasites have been reported for virtually every anti-parasitic therapeutic in current use (Poulin, 2007). Much like bacteria, parasites employ many mechanisms to develop drug resistance, including genetic mutations that result in insensitive or overexpressed target enzymes and proteins, altered metabolism, expression of drug efflux pumps, and epigenetic changes (Sharma et al., 2013).

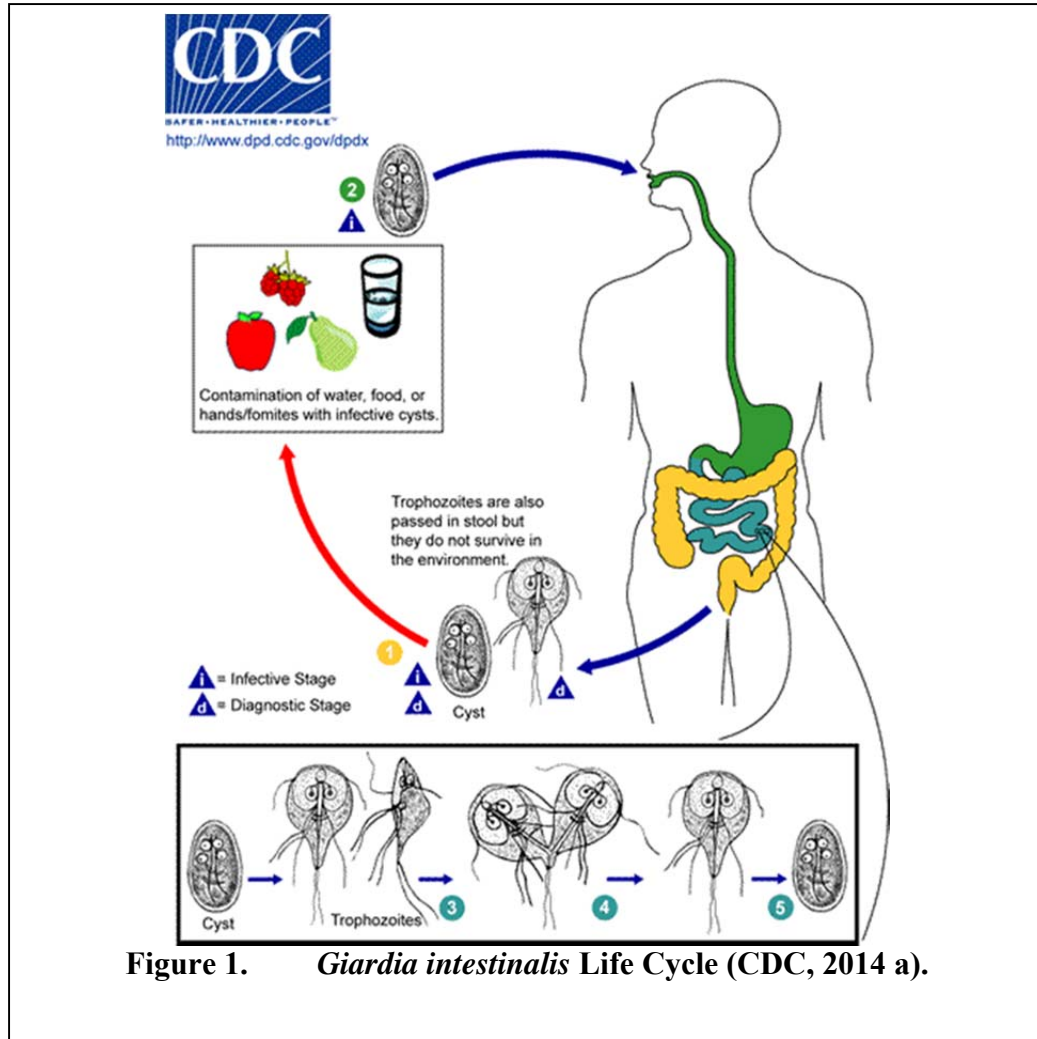
Whatever the mechanism, the result is the same. Drugs that were extremely time consuming and expensive to produce are now ineffective in treating certain strains of parasites. Alexander Fleming, the discoverer of penicillin, argued in 1946 that chemotherapeutic drugs capable of sustained activity against microbes were unlikely due to their inherent ability to mutate rapidly and acquire resistance (Fleming, 1946; Alekshun & Levy, 2007). Thus, there is a continual need to rapidly and cheaply identify new antibiotics. Recent research has begun to explore the development of antibiotics that modulate pathogen growth and virulence, without creating a strong selective pressure for drug resistance that typically accompanies cytotoxic drugs. This, along with drug rotation, combination drug therapy, and appropriate antibiotic use should result in longer periods of drug effectiveness (Davies & Davies, 2010).

Giardia intestinalis

Giardia intestinalis (sometimes referred to as *G. duodenalis* or *G. lamblia*) is a parasite of the phylum Protozoa, order Diplomonadida. As seen in Figure 1, *Giardia intestinalis* exists as a motile single-celled trophozoite inside the host intestinal tract. The

trophozoite has a 12-15 μm long dorso-ventrally flattened body that is convex on the dorsal surface. The dorsal surface also contains a bi-lobed adhesive disc used to attach to the surface of host cells lining the intestinal wall. *Giardia* is unusual in that it contains two nuclei behind the lobes of the adhesive disks, thus conferring tetraploidy and giving the trophozoite its distinctive “bespectacled” look when viewed under the microscope. *Giardia* lacks other organelles such as Golgi bodies, lysosomes, and smooth endoplasmic reticulum, but does develop four pairs of flagella that allow rapid movement when unattached from the intestinal wall. *Giardia* is also amitochondriate and lacks respiratory metabolism. Instead it relies on anaerobic fermentation and salvage of host nutrients to supply its metabolic needs (Roberts & Janovy, 2013).

Giardia infections begin by ingestion of heavily walled parasite cysts. Once in a new host, stomach acid and digestive enzymes begin to degrade the parasite cyst wall. In the duodenum, the organism completes excystation and two new flagellated trophozoites emerge to establish an infection in the duodenum and jejunum. The trophozoites attach to the intestinal mucosal lining through the ventral adhesive disks and absorb nutrients from intestinal cell exudates and luminal contents. The infection proceeds as the trophozoites replicate by binary fission. Unattached trophozoites migrate to the drier stool of the colon where they encyst in a process that envelopes the trophozoite in protective fibers. The hardened cysts are then excreted by the host and transmitted to the next host through fecal contamination of food or water (Roberts & Janovy, 2013).



Because *Giardia* attaches to the lining of the small intestine in the host, the most common symptoms of infection are chronic diarrhea, greasy stool, foul smelling flatulence, intestinal cramping, rectal fissures, and weight loss (Ali & Hill, 2003). In healthy adults with robust immune systems the infection may be asymptomatic. This can lead to unknowing transmission of the disease to close contacts (Thompson, 2000). *Giardia* is rarely fatal but severe disease does occur. In most cases of severe disease, the victims are commonly immune-compromised individuals, children under age 5, or pregnant women (Teunis, Medema, Schets, & Havelaar, 1998). Since *Giardia* is the

leading cause of reported outbreaks of waterborne illness in the United States, it remains a significant widespread health hazard (Lengerich, Addiss, & Juranek, 1994).

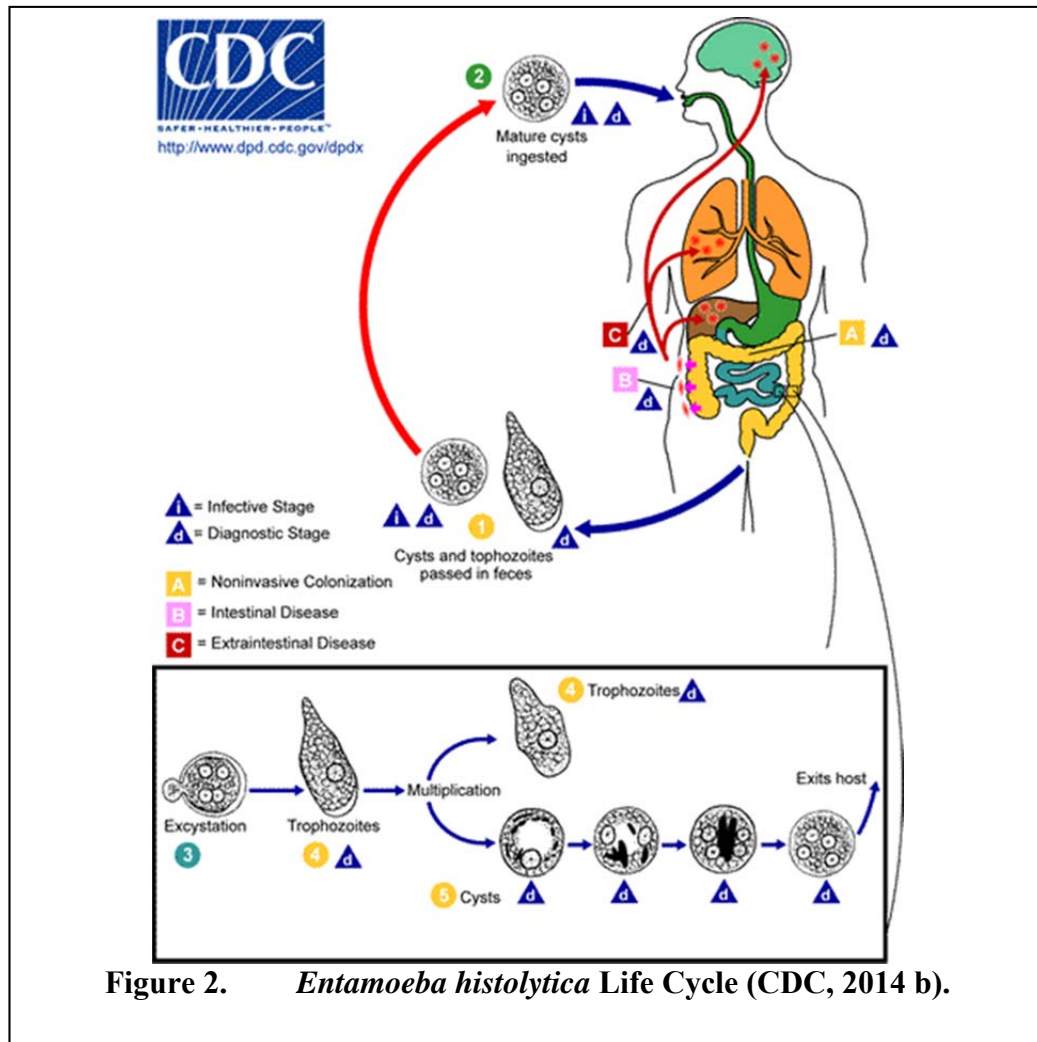
According to recent CDC estimates, the annual incidence of giardiasis was estimated at > 1.2 million cases in the United States alone (Scallan et al., 2011). Worldwide infection rates are estimated at over a billion cases annually (Auerbach, 2007). Even in places where water quality is heavily regulated, outbreaks still occur due to the extreme toughness of the cysts, which resist killing by chlorination and UV irradiation (Isaac-Renton, Cordeiro, Sarafis, & Shahriari, 1993). True preventative measures require filtration mechanisms that can exclude particles larger than 10 μm . In some instances, even these precautions fail to fully decontaminate water supplies (LeChevallier, Norton, & Lee, 1991a, b).

The primary treatment for giardiasis is the nitroimidazole drug metronidazole. The standard daily oral dose for treatment of giardiasis is 500 to 750 mg for five to ten days (National Toxicology Program, 2011). Metronidazole is believed to be a human carcinogen because experiments in rats and mice have shown that oral treatment with metronidazole increases rates of tumor formation (National Toxicology Program, 2011). Other treatments such as albendazole and tinidazole are also used, but have been reported to be either mutagenic or teratogenic (Abboud et al., 2001; Karabay et al., 2004). Considering that the most common sufferers of giardiasis are young children and pregnant women, these side effects are unacceptable. For this reason, along with the emergence of metronidazole resistant isolates of *Giardia intestinalis* and the common recurrence of disease in previously treated patients, the need for a new drug treatment regimen is at an all-time high.

Entamoeba histolytica

Entamoeba histolytica is a parasite of the phylum Protozoa, order Lobosea.

Inside the host gastrointestinal tract, *E. histolytica* exists as a 10-60 μm long trophozoite with short, blunt pseudopodia for locomotion. Like *Giardia*, *E. histolytica* cells are amitochondriate and lack respiratory metabolism. The cytoplasmic membranes are quite thin and clear, which allows for visualization of the nucleus and endosomes after staining. Food vacuoles often contain host erythrocytes, which are darker than the surrounding endoplasm and make the cells look like chocolate chip cookies (Figure 2).



Similar to *Giardia*, infection by *Entamoeba* begins with ingestion of cysts. The major source of infectious cysts is fecal contaminated food and drinking water. Other sources include anal sex and overcrowded, unhygienic living conditions (Walsh, 1986). Inside the host, *E. histolytica* excyst to form trophozoites that colonize the large intestine. Trophozoites divide by rapid binary fission into four daughter trophozoite cells. In asymptomatic patients, some trophozoites migrate to the drier stool of the colon where encystation occurs. Cysts are subsequently shed in the stool.

If untreated, *Entamoeba histolytica* causes amoebiasis. The most common symptoms of infection are chronic bloody diarrhea, cramps, and vomiting (Roberts & Janovy, 2013). Asymptomatic disease is common. The parasite can invade the tissues of the cecum, leading to tissue ulceration and migration via the blood stream to other host organs (mainly liver, lung, and brain), where it can further invade to cause potentially fatal abscesses and tissue necrosis (Roberts & Janovy, 2013).

Amoebiasis can also be fatal when the host suffers acute dysentery leading to extreme dehydration. The victim is usually an otherwise healthy young man who delays seeking treatment until the symptoms become unbearable. In other cases of death, the victims are usually the very young, the very old, or the immunocompromised. In total, approximately 50-100,000 people die every year from amoebiasis, which makes it second only to malaria as the leading cause of death due to parasites (Stanley, 2003).

Like giardiasis, metronidazole is the most common treatment for amoebiasis. The standard oral dose for treatment of amoebiasis is only slightly lower than the dose that has been shown to cause tumors in mice and rats (Roberts & Janovy, 2013). Increasing reports of metronidazole treatment failure suggest drug resistance has begun to develop in

E. histolytica (Bansal, Malla, & Mahajan, 2006). Albendazole has been used effectively to treat metronidazole resistant amoebiasis. However, albendazole is a known teratogen and is contra-indicated in the treatment of amoebiasis in pregnant women (Venkatesan, 1998; Abboud et al., 2001; Karabay et al., 2004). A vaccine against amoebiasis has been tested in animals, but has yet to be approved for use in humans (Stanley, 2006).

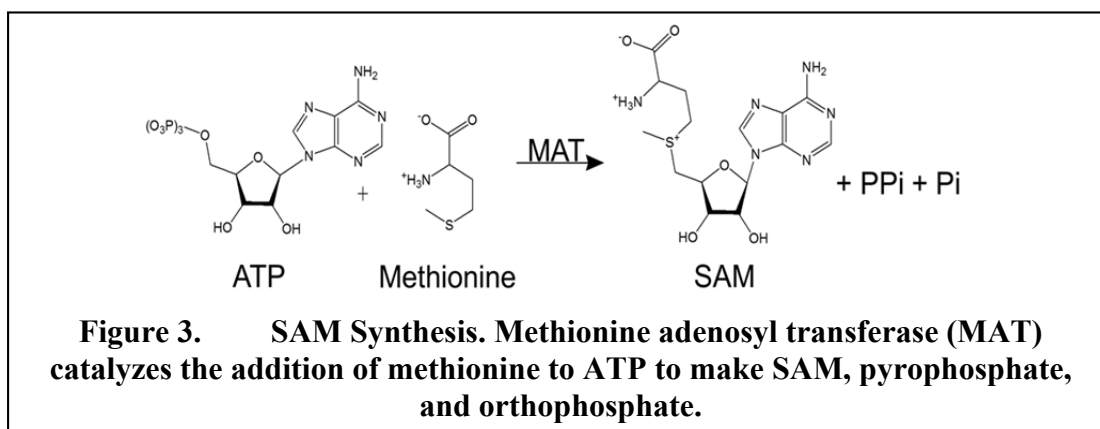
Unfortunately, the lack of sustained immunity following native infection suggests that the development of a successful vaccine will be difficult (Haque et al., 2006), and further supports the need to develop additional therapeutics to treat amoebiasis.

Methionine, SAM Reactions, and the Methionine Salvage Pathway

Methionine is an extremely important amino acid for all cells due to its role in a variety of biochemical reactions including protein synthesis, the synthesis of other amino acids through trans-sulfuration reactions, and the creation of S-adenosylmethionine (Nozaki, Ali, & Tokoro, 2005). Parasites (like humans) do not make sufficient methionine to meet their metabolic needs, thus it is termed an “essential” amino acid (Huxtable, 1986). In parasites, widespread methionine auxotrophy sponsors both methionine scavenging systems from the host, as well as salvage pathways to recycle the sulfur containing amino acid (Marr & Müller, 1995).

The majority of methionine is used to create S-adenosylmethionine (SAM, AdoMet) from ATP using the enzyme methionine-adenosyl transferase (MAT, or SAM synthase) (Figure 3). SAM is an activated nucleoside that is a source of chemical groups used in hundreds of biochemical reactions, including methylation reactions, polyamine synthesis, and radical SAM reactions (Fontecave, Atta, & Mulliez, 2004). Byproducts of these reactions consist of adenine nucleosides from which salvage of both the methionyl

sulfur and purine base are important due to the underlying auxotrophy for these compounds in the protozoan parasites like *G. intestinalis* and *E. histolytica*.



The primary role of SAM is to serve as a methyl group donor in a wide array of transmethylation reactions used to modify cellular DNA, proteins, and other small molecules (Figure 4). S-Adenosylhomocysteine (SAH, AdoHcy) is produced as a byproduct of the reaction (Chiang et al., 1996; Fontecave et al., 2004; Grillo & Colombatto, 2005). Transmethylation reactions play a critical role in a variety of cellular processes including the regulation of gene expression, proper assembly of membrane constituents, and protein-protein interactions. SAH is a product inhibitor of transmethylation reactions, and is catabolized efficiently to prevent intracellular accumulation (Kloor & Oswald, 2004; Hall & Ho, 2006). Two enzymes are of major interest for interruption of methionine salvage and SAM recycling in target organisms: SAH hydrolase (SAHH) and MTA nucleosidase (MTN).

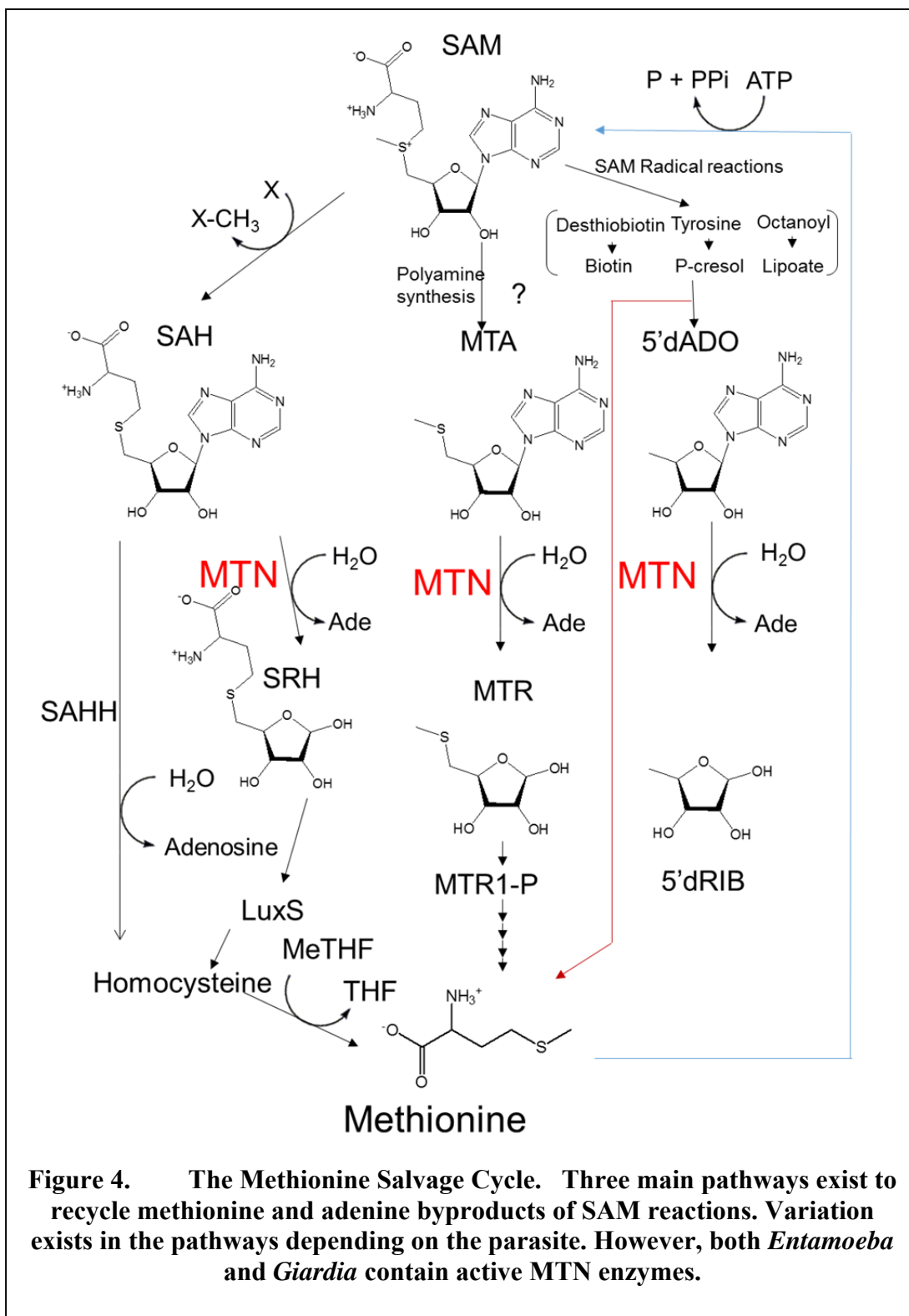
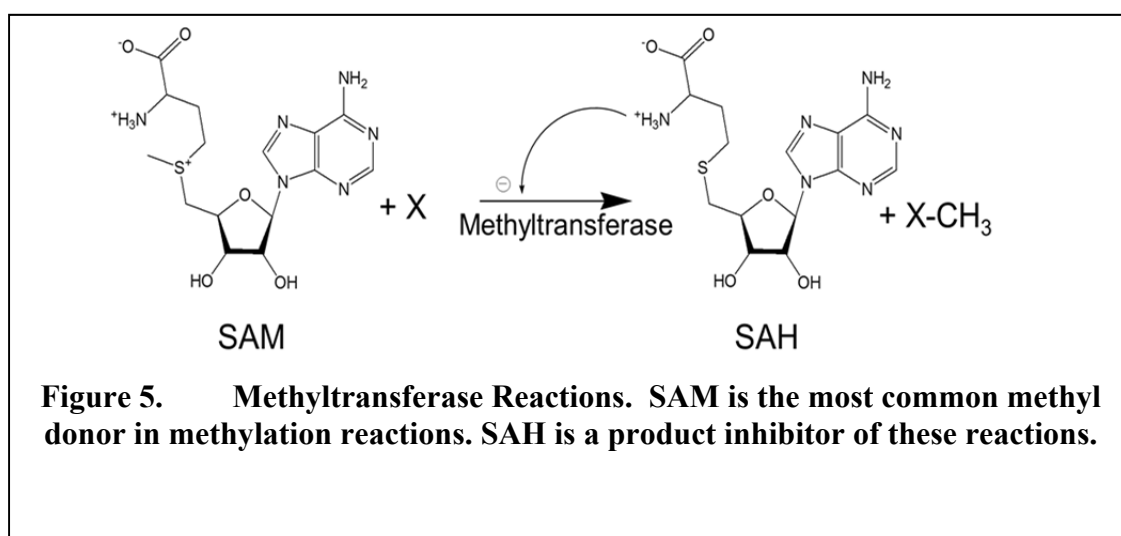


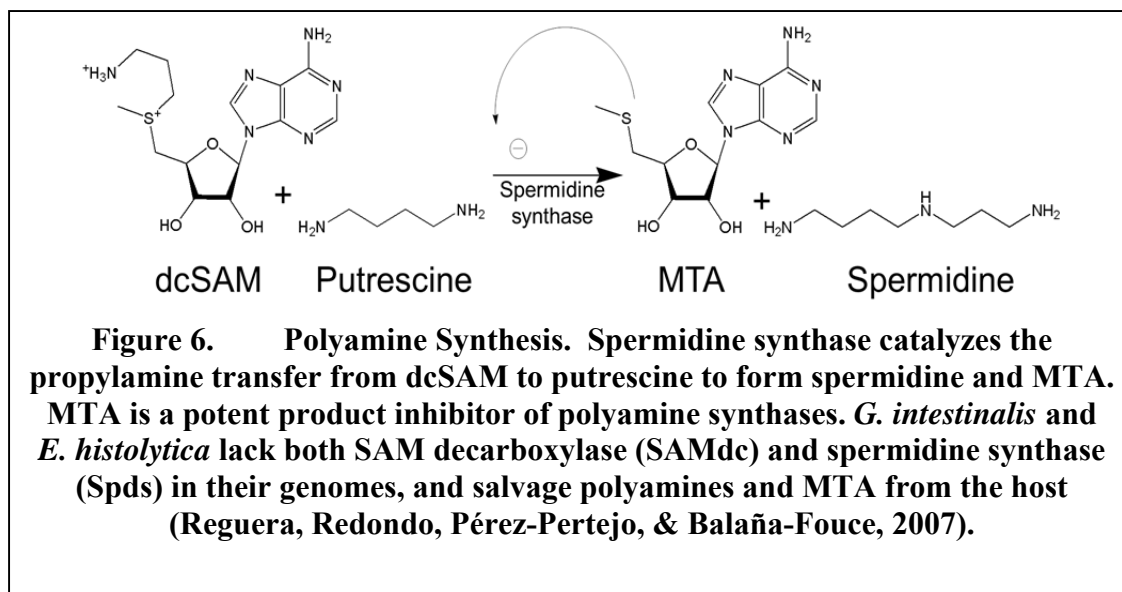
Figure 4. The Methionine Salvage Cycle. Three main pathways exist to recycle methionine and adenine byproducts of SAM reactions. Variation exists in the pathways depending on the parasite. However, both *Entamoeba* and *Giardia* contain active MTN enzymes.

SAM reactions are crucial for parasite replication and thus inhibition of SAM production or recycling would result in stunted growth, making enzymes related to SAM pathways attractive targets for drug development (Parker et al., 2003). SAHH catabolizes S-adenosylhomocysteine (SAH). SAHH inhibition would cause intracellular SAH accumulation, in turn leading to feedback inhibition of methylation reactions (Figure 5). Inhibition of methylation reactions would impair DNA replication and can trigger apoptosis (Parker et al., 2003; Gopisetty, Ramachandran, & Singal, 2005). Thus, SAHH inhibition is a tempting target for new drug development. Indeed, some success has been found with carbocyclic 3-deazaadenosine, an SAHH inhibitor that has shown promise as an antiviral drug against Ebola infections in mice (Huggins, Zhang, & Bray, 1999). Unfortunately, the SAHH enzymes present in both humans and parasites bear a striking structural homology, which would make the selective targeting of parasite SAHH extremely difficult. Thus far, no inhibitors of parasite SAHH have been found that could act as broad spectrum anti-parasitic drugs while leaving the human SAHH unaffected (Parker et al., 2003; Minotto, Ko, Edwards, & Bagnara, 1998).



Methylthioadenosine Nucleosidase (MTN): A New Drug Target

In plants and many microbes, the enzyme methylthioadenosine nucleosidase (MTN) catabolizes MTA to MTR and adenine (Figure 4). MTA is the product of polyamine synthesis (spermidine, spermine) that utilizes decarboxylated SAM as a propylamine donor (Figure 6). Polyamines are important for DNA replication and cell proliferation. MTA is a potent product inhibitor of polyamine synthesis, and is cytotoxic when it accumulates in the cell. Since MTN is not found in mammalian cells, it is a possible target for chemotherapeutic agents (Riscoe, Ferro, & Fitchen, 1989; Walker & Barrett, 1997). Instead, mammals have MTA phosphorylase (MTAP), which works on the same substrate but has different enzymatic binding properties that may be exploitable for development of selective MTN-specific antibiotics (Lee et al., 2004).



One other pathway of note involves the use of SAM as an oxidizing agent in radical reactions. The radical SAM enzymes reduce the sulfonium on SAM via a coordinated iron-sulfur cluster (Jarrett, 2003; Challand et al., 2009) to create methionine

and 5'-deoxyadenosine (5'-dADO) radical, which then abstracts hydrogen from any nearby substrate with a C-H bond (Figure 7) (Igarashi & Kashiwagi, 2010). The substrates vary and usually result in anaerobic oxidations, sulfur insertions, isomerizations, ring formations, and other unusual methylations (Jarrett, 2003; Parveen & Cornell, 2011). Members of the radical SAM superfamily of enzymes, including biotin synthase, lipoyl synthase, and tyrosine synthase, were all product inhibited by 5'-dADO and methionine (Challand et al., 2009). The activity of SAM superfamily enzymes was restored when MTN was added to the assays. Thus, inhibition of MTN that catabolizes 5'-dADO to adenine and 5-deoxyribose is likely to ultimately lead to product inhibition of these radical SAM enzymes. This could lead to depletion of the biotin, lipoate, and thiamine cofactors required for numerous metabolic enzymes in the cell, and impairment of central carbon metabolism (Parveen & Cornell, 2011). There are about forty known radical SAM reactions that are necessary for the cell (Jarrett, 2005; Frey, Hegeman, & Ruzicka, 2008). While it is not known if product inhibition is universal, the fact that it occurs in some radical SAM reactions makes MTN an even better drug target.

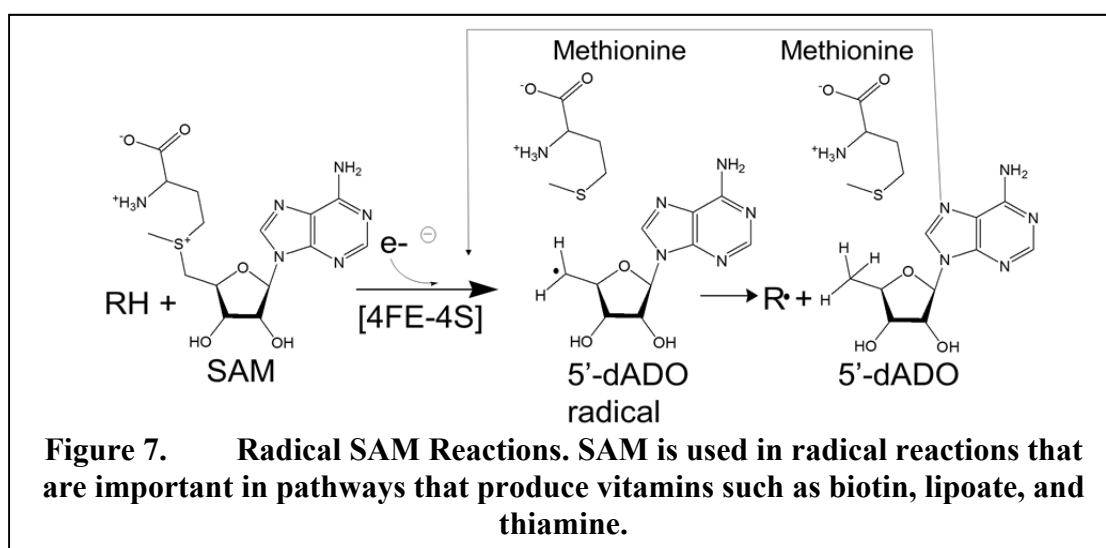
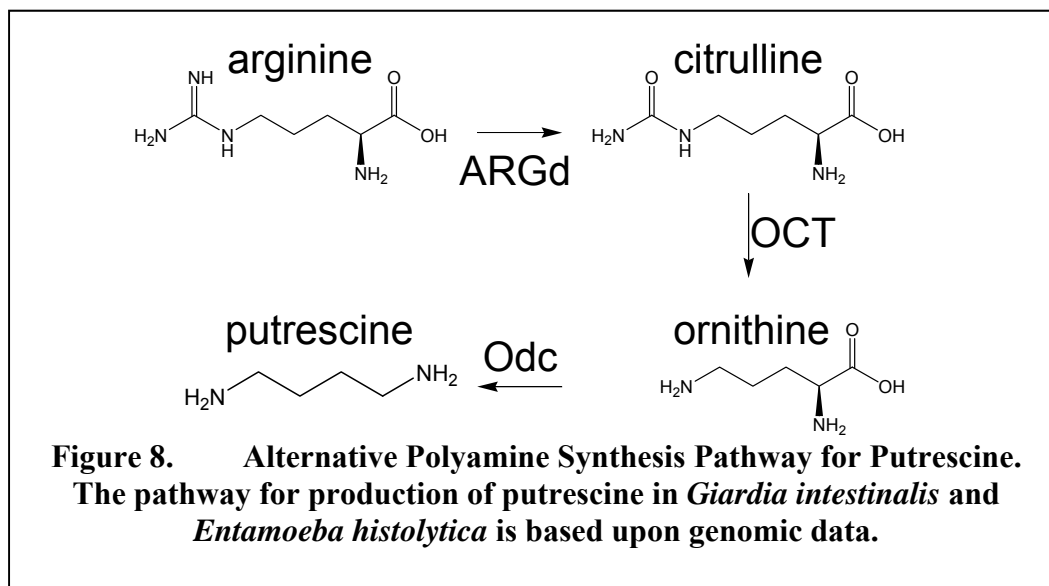


Figure 7. Radical SAM Reactions. SAM is used in radical reactions that are important in pathways that produce vitamins such as biotin, lipoate, and thiamine.

The methionine salvage pathways of the parasitic protozoa studied here are more complicated than the general bacterial pathway. Analysis of the publically available *Giardia intestinalis* genomes reveals the presence of two MTN genes, but not SAHH genes. This is contrary to a previous report that *Giardia intestinalis* contained a standalone SAHH (Riscoe et al., 1989). Thus the *Giardia* MTNs should act like bacterial MTNs and catabolize all three nucleosides: MTA, SAH, and 5'-dADO. This suggests that MTN inhibition will target methionine and purine salvage from three substrates: SAH, MTA, and 5'-dADO. In contrast to *Giardia*, the *Entamoeba histolytica* genome contains the genes for SAHH and MTN, and thus catabolizes SAH to adenosine and homocysteine, while only MTA and 5'dAdo are degraded by MTN.

Genomic analysis also reveals that *Giardia* and *Entamoeba* lack SAM decarboxylase and spermidine synthase, but instead have a separate polyamine synthetic pathway that may be specific to anaerobic protozoan parasites. In this alternate pathway, arginine is converted by arginine deiminase (ARGd) to citrulline that is then converted by ornithine carbonyl transferase (OCT) to ornithine, which is then converted by ornithine decarboxylase (Odc) to putrescine (Figure 8). Indeed, in these parasites putrescine is the predominant polyamine, while spermidine and spermine are in low concentration and probably originate from the host (Marr & Müller, 1995; Reguera, Tekwani, & Balaña-Fouce, 2005). This revelation raises the question as to the source of MTA within the parasites, since they appear to lack SAM decarboxylase and spermidine synthase. It would appear that the answer may be found in the presence of a MTA P2 transporter in parasites that is capable of transporting MTA from the host (Goldberg, Rattendi, Lloyd, Sufrin, & Bacchi, 2001).



These deviations from the prototypical polyamine pathway are not unexpected. After all, protozoa are a very large and disparate group of organisms with at least 500 million years of divergent evolution in metabolic pathways to accommodate differences in host, life cycle, and location of colonization. As such, it is imperative that present studies focus on the constructed genomes of each organism to gain a full understanding of which enzymes are present in order to identify better drug targets within those pathways that will lead to the development of better drugs.

Inspection of the parasite genomes in this study revealed that MTN is an essential enzyme for purine salvage. Alignments of *E. coli* and parasite MTN primary sequence (Figure 9) show that the active site residues in the MTN enzymes are highly conserved. A greater than 68% homology was found between all the target MTN enzymes, while significant homology was not found with the human MTAP enzyme. This suggests that it could be possible to develop drugs that would work as broad spectrum antibiotics by inhibiting MTNs in both parasites, but not cross react with human MTAP.


```

EC      -----MKIGIIGAMEEIVTLIRDKIEN
GI MTN-1 MLVSKERRTAPVFVVIIPMPTIFHAFKLQD
GI MTN-2 -----MSSQKRIICAMCALERBFGMKKCFEK
EH      -----MIICILAPMKEILQATCDKYPO
MTAP    --MASGTTTAVKICIIIGGTGLDDPEILEGRTE

EC      ---RQTISLGGCEIYTGQINGTEVALL-KSIG
GI MTN-1 KESYKEEVIAGRKYFTKLEKYTLVLC-ECIG
GI MTN-2 E--LQSEDHCGRTFYTGELSGQTVVIS-KSIG
EH      ---STMLEKCGIHYHYKIKDNEIILM-OCVVG
MTAP    KYVDPFPGKPSDALILGKIKNVDCVLLARHGRQ

EC      -----KVAALGATLLEHCKPDVINTGSAG
GI MTN-1 -----KVCSGTAAVLLDHFNADVIVAAGVAG
GI MTN-2 -----KVAASTAAMI SVFGCSEVIFLGVAG
EH      -----KVNAALAVSTIKHLFNVDIILNLSGAC
MTAP    HTIMPSKVNY-QANIWALKEEGCTHVIVTTACG

EC      GLAPTLKVGDIVVDSDEARYHDAD-VTAFGYE--
GI MTN-1 GLKEGIAIGDIVVDSVMOHDFN-CYFPVPRHT
GI MTN-2 GIQGRAAIGDIVVSTAIIQHDFD-GRPWWERSV
EH      GMKLGQKPLDIVIGTELVTVDV-ITPLGFA--
MTAP    SLREELQPGDIVIIDQFIDRTTMRPQSFYDGS

EC      ---YEQ--LPGCP-----AGFKADDKLI
GI MTN-1 IVNIQVDVMHADKALTTTLOGIAEEFLKKNYST
GI MTN-2 VFSVQKCEIIPADGQLQTRAQAAVQAVLADMAL
EH      ---YQE--LLGEP-----KSWFSDKELV
MTAP    SCARVCHIPMAEPFCP-----KTREV

EC      -----AAAEACIAELNNAVRLIVSGDA
GI MTN-1 IVP-----P-CV-RETHGLSWPRLHVGCSISGDK
GI MTN-2 VLDDNSEPIGRRILAQLNRSFKLLTGSVLSGDDQ
EH      -----SLATKCSSSDDLPTIHYGTIGTSDA
MTAP    LIE-TAKKLG--LRCHSKGTM-----VTIEGDR

EC      FINGSVGLAKIRHNF-PQAI AVEEATAIAHV
GI MTN-1 FLENVDEKMELIKRI-PAALVIEEGGAVGQVC
GI MTN-2 FVSSDEMKNELGSRF-ESALCVEEGAAVAQIC
EH      FVSAPMVQS-IQNKFDNRIVCAEIEGCAVAHSC
MTAP    FSSRAESFM--FRTW--GADVINMTVPEVFLA

EC      HNFNVPFVVRAISDVAD-QL--SHLSFDEFLA
GI MTN-1 YEASKPFVSLRIVSDLCD-GN--GLDNYDAYCT
GI MTN-2 YEARVPYIIIRAISDSGS-GE--ATVDFEFCN
EH      TKLGI RFI VTRSLSDVPS-EDGKSHEKMMDYLS
MTAP    KEAGICYASTAMATDYDCWKHEEAVSVDRVLK

EC      VA---AKQSSLMVESLVQKLAHG-----
GI MTN-1 HV---ASK--VLYAILSSFFAQVA-----
GI MTN-2 GI---SSP--LMLAVLKSYLASASKFDYCA--
EH      RA---SHNASILVSRILIEQLIVN-----
MTAP    TLKENANKAKSLLLTIP---QIGSTEWSETL

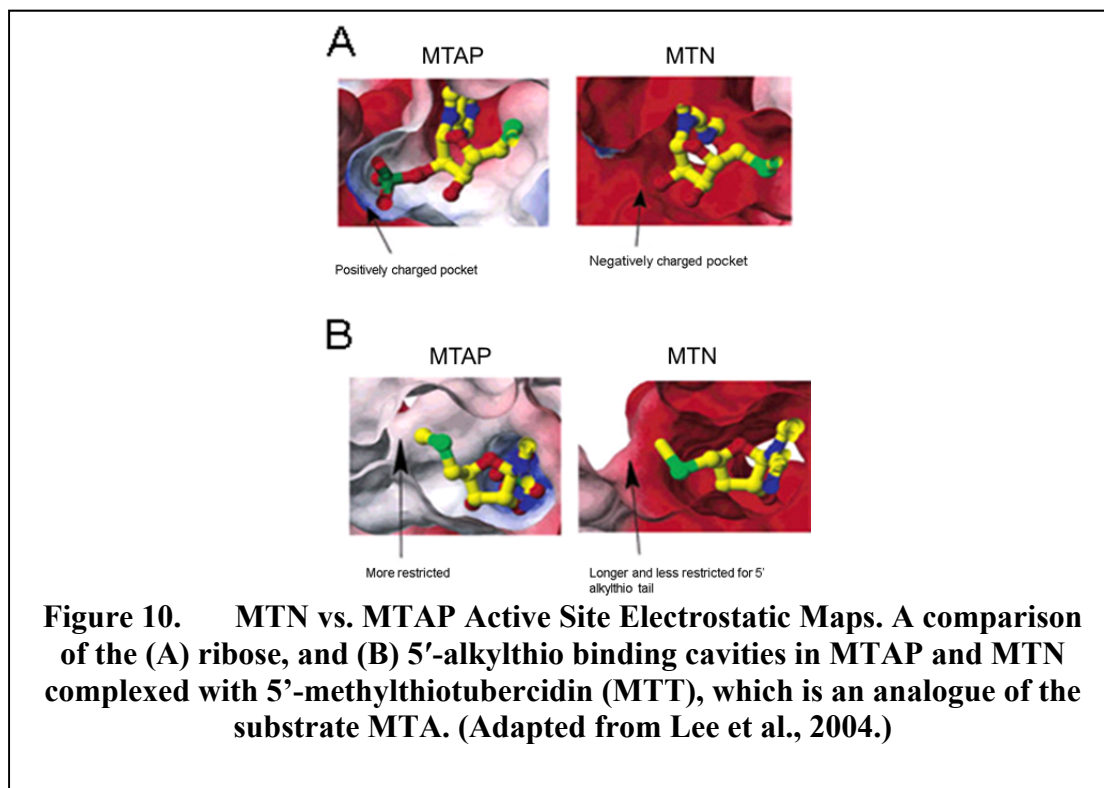
EC      -----
GI MTN-1 -----
GI MTN-2 MSALIMIQFSIRCRHLTQRSPME-----
EH      -----
MTAP    HNLKNMAQSFVLLPRH-----

```

Figure 9. Clustal W Alignment of MTN Sequences. Sequence comparison of microbial MTNs to human methylthioadenosine phosphorylase (MTAP) is shown. Homologous residues are shaded. Catalytic amino acids are shaded in black. Amino acid homologies to *EC MTA nucleosidase* are as follows: 86% to *EH*; 77% to *GI MTN-1*; and 68% to *GI MTN-2*.

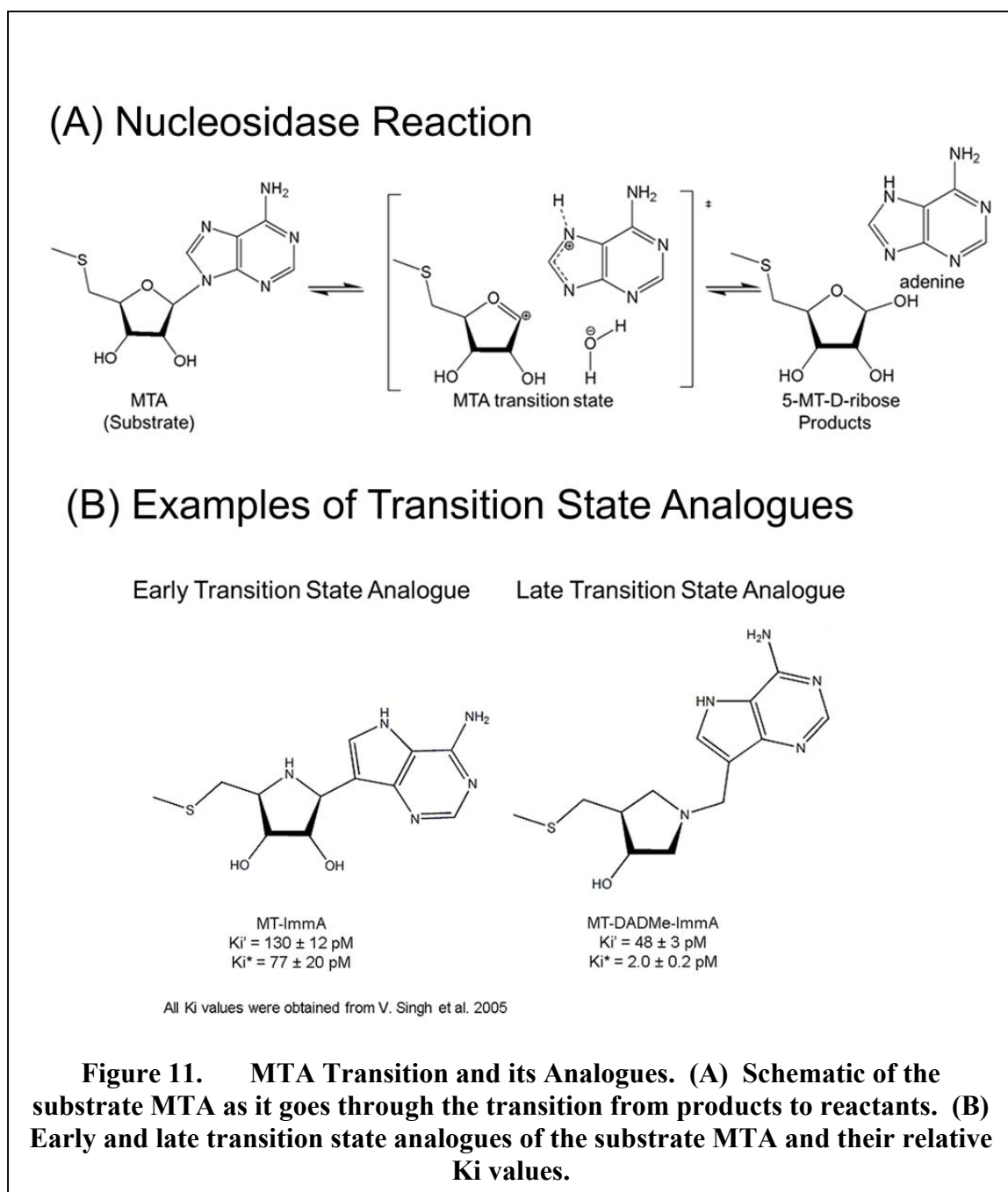
While MTNs have conserved active site residues, they also have differences in the active site that set them apart from human MTAP, and that may be exploitable for drug design. For example, the substrate 2' hydroxy binding pocket electrostatics in MTAP is

positively charged, while it is negatively charged in MTNs (Figure 10, part A). Likewise, the 5'-alkylthio binding cavity of the MTNs is more extended and open than that found in the MTAP active site (Figure 10, part B). Thus, a drug that bears a positive charge at the 2' hydroxy position of the ribose and a larger 5'-alkylthio chain would likely discriminate between the MTNs and human MTAP (Lee, Cornell, Riscoe, & Howell, 2003).



MTN inhibitors have been created based on the transition states of the substrate MTA as it is cleaved to MTR and adenine. A transition state is an unstable structure that occurs between the chemical structure of the substrate and the products of a reaction. Transition states exist for only about 10^{-13} sec and thus there is no way to directly observe the structure of a transition state. However, it is known that enzymes bind tighter to the transition state than they do to the substrate. Thus, transition state analogues (TSAs) should make better inhibitors than mimics of the substrate (Schramm, 1998). An

extensive body of work to create and test these TSAs has been reported by Dr. Vern Schramm's lab (Albert Einstein College) (Schramm 1998; Schramm et al., 2008; Singh et al., 2004; Singh et al., 2005; Singh, Lee, Núñez, Howell, & Schramm, 2005; Guitierrez et al., 2009). These inhibitors, based upon the MTA transition state, are designed to bind with a higher affinity than that of the native substrates (Figure 11, part A). The substitution of large groups at the 5'-alkylthio position improves specificity. The TSAs show extraordinary tight binding affinities for *E. coli* MTN, yielding K_i values ranging from picomolar to femtomolar concentrations. Of note, even greater binding affinity was found when the drug was designed to mimic the late transition state by extending the bonds between the nitrogen on the ribose and the purine ring. This yielded K_i values into the femtomolar level (Figure 9, Part B) (Singh, Lee, et al., 2005).



Unfortunately, these TSAs have not proved to be particularly effective as antibiotics against *E. coli*, showing only modest IC_{50} values, which only went as low as the micro molar range (Gutierrez et al., 2009). However, Gutierrez et al. (2009) did show the ability of TSAs to block quorum sensing and reduce biofilm production that are

important virulence factors. Transport of these drugs into the cell may be a limiting factor in their poor performance on *E. coli* (Longshaw et al., 2010). Interestingly, pathogens like *Borrelia burgdorferi*, which are purine auxotrophs, showed a much greater sensitivity to MTN inhibitors (Cornell, Primus, Martinez, & Parveen, 2009). The cause of this increased sensitivity could be due to the fact that these organisms are more reliant on the salvage of methionine and purines that could make them more susceptible to MTN inhibition (Cornell et al., 2009).

In-silico Computational Drug Discovery

Historically, drugs were discovered either serendipitously (like Penicillin) or by looking closely at a folk remedy to find the active ingredient (like salicylic acid from willow bark) (Houbraken, Frisvad, & Samson, 2011; Sneader, 2000). The drug discoverers did not know how these drugs worked at first. They were limited by an inability to see the mechanisms of pathogenesis at work in a disease process or the drug reaction mechanisms. However, they could make better drugs by implementing small chemical changes to known drugs and monitoring the results.

In 1958, the first X-ray crystallographic structure for myoglobin was reported (Kendrew et al., 1958). Since that time, X-ray crystallography has been used to examine thousands of structures of proteins in the presence or absence of bound substrate or other ligands. This has allowed enzyme reaction mechanisms to be viewed for the first time, and expanded the ability of scientists to rationally design drugs.

By the mid 1980s, computer renderings of bio-molecules from X-ray crystallography, NMR, or homology modeling were beginning to be widely available. These could be manipulated and the free energy measured for theoretically bound

ligands. This further opened the window for the rational design of drugs (Anderson, 2003). This process has come to be called structure based drug design or *in-silico* based drug design (Anderson, 2003; Jorgensen, 2004). Some success with this method was reported as early as 1990 with the discovery of human immunodeficiency virus (HIV) protease inhibitors (Roberts et al., 1990; Erickson et al., 1990). In the early years, the method was limited by the difficulty of attaining drug-binding affinities through computational measurement that were in good agreement with the experimental data (Salemme, Spurlino, & Bone, 1970). By 2009, however, *in-silico* drug screening approaches were responsible for finding anti-HIV fullerene derivatized amino acids that had computational binding scores with HIV-1 protease that were within 10% of experimental binding energies (Durdagi et al., 2009).

As computer modeling of biomolecules has improved, the composition of computational drug lead libraries has also advanced. In 2006, small molecule databases were used to custom build inhibitors to HIV-1 integrase (Jaganatharaja & Gowthaman, 2006). The use of chemical fragment libraries, which greatly increase the variety of chemical possibilities and therefore greatly increases the hit rate for new drug leads, has become a major contributor to the speed and ease of novel drug discovery (Hajduk & Greer, 2007). By 2014, *in-silico* methods have become so reliable that they were used to identify allosteric inhibitors of HIV-1 protease (Kunze et al., 2014).

In order to accomplish new drug discovery from x-ray crystallographic structures, a reliable assay to monitor the bio-molecular process is needed. With the best estimation of the binding site free energy, protein structure, and automated physical screenings utilizing pre-synthesized drug libraries, high throughput screening (HTS) processes have

been developed to identify new drugs. HTS allows large numbers ($\sim 10^5$) of chemical compounds to be examined for “lead discovery” (Terstappen & Reggiani, 2001).

The use of *in-silico* methods and HTS has a proven track record in development of drugs against HIV (HIV protease inhibitors, etc.) and cancer (Gleevec) (Hajduk & Greer, 2007). But use of this technology is not limited to these diseases. In fact, any disease with a known macromolecular target would make a good candidate for this type of drug discovery method, and this is precisely why this approach was used in our study. Since there are homology models of *Giardia* and *Entamoeba* MTN's (to *E. coli* MTN) available for computational manipulation, it is logical to employ *in-silico* methods to find new drug leads to inhibit their action. This is the approach our collaborator, Dr. Danny Xu (Idaho State University, School of Pharmacy), took to identify a set of potential MTN inhibitors. He used *in-silico* drug discovery methods to screen compounds in the NCI Diversity Set II small molecule library against known *E. coli* MTN crystallographic structures, and homology models of *E. histolytica* and *G. intestinalis* MTNs. Free energy calculations of drugs were used to identify thirty-three compounds with favorable binding into MTN active sites. Examples of three lead compounds bound to the active site of *E. coli* MTN are shown in Figure 12. The structures show extensive interactions between the compounds and the active site residues known to be involved in catalysis (e.g., Glu12, Asp197, etc.).

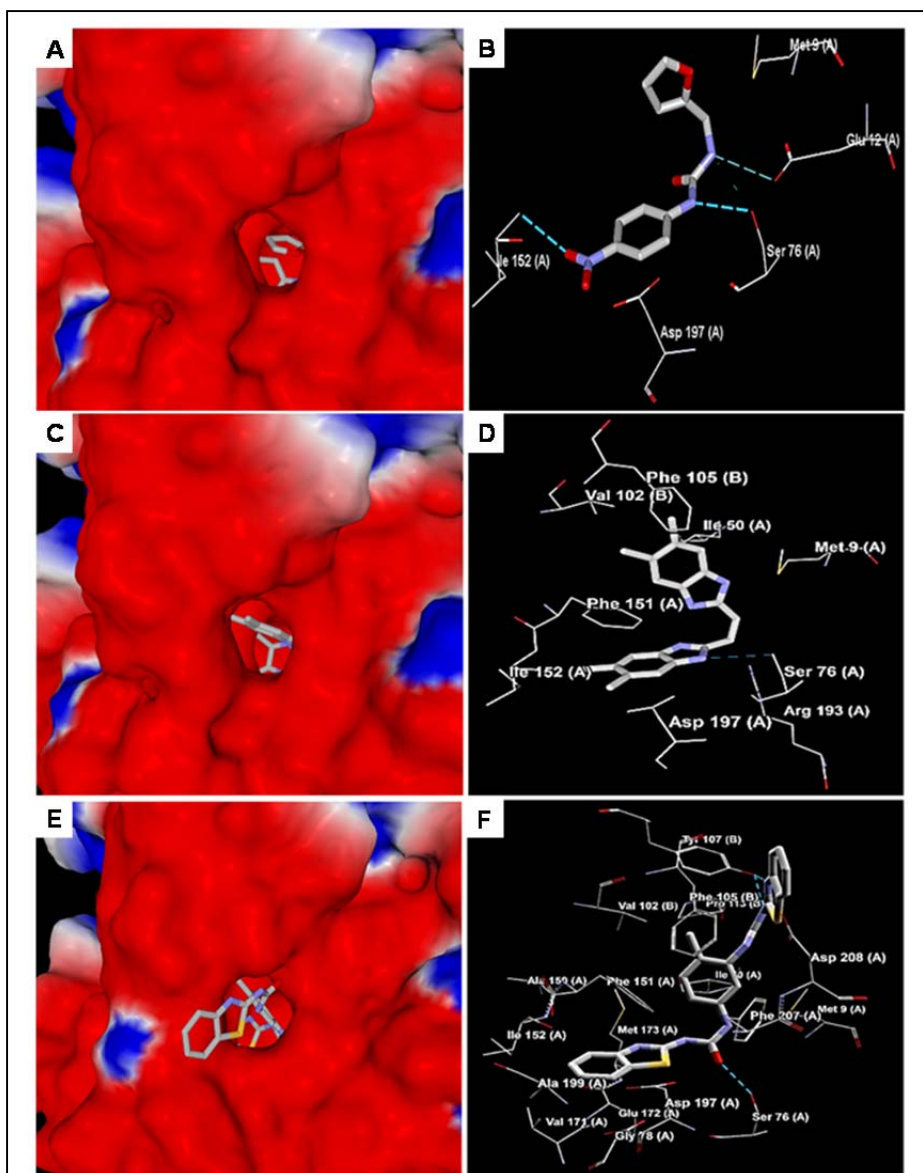


Figure 12. *E. coli* MTN Active Site Electrostatic Maps with Bound Inhibitors. Box A and B show inhibitor 5A, C and D show drug 15A and E and F show drug 27A bound.

Summary

MTN is a necessary enzyme for *Giardia* and *Entamoeba* metabolism and is thus an excellent target for novel anti-parasitic drugs. Inhibition of MTN causes accumulations of SAH, MTA, and 5'dADO, which negatively impacts SAM metabolic pathways. The inability to salvage methionine and purines, and the resulting impairment to SAM pathways, likely causes parasite cell death due to nutrient depletions and interruption of energy metabolism. While previously reported bactericidal activity of MTN inhibitors is modest, their ability to modulate virulence in these pathogens shows that it has potential as a broad spectrum treatment (Knippel, 2013).

In the following chapters, thirty-three potential MTN inhibitors found through *in-silico* methods were analyzed for *in vitro* activity in enzymes and cell proliferation assays. The inhibitors were tested using a spectrophotometric enzyme assay against *E. coli* MTN, *G. intestinalis* MTN-1, *G. intestinalis* MTN-2, *E. histolytica* MTN, and human MTAP. The inhibitors were also tested for *in vitro* anti-parasitic activity against *G. intestinalis* trophozoites in resazurin reduction and BacTiter-Glo™ assays, and for anti-proliferative activity against human Hela and Jurkat cell lines using the resazurin reduction assay. These tests identified four drug lead compounds that showed low micromolar to submicromolar affinities for parasite MTNs, and inhibited 50% of *Giardia* growth at concentrations of 10-90 micromolar. Furthermore, several of the compounds could effectively discriminate between the parasite MTNs and human MTAPs. The results of this work show that four inhibitors were identified that are potential lead compounds and support their further drug development.

CHAPTER TWO: MATERIALS AND METHODS

Induction and Purification of Recombinant Enzymes

The genes encoding *Giardia* MTN-1, *Giardia* MTN-2, and *Entamoeba* MTN were amplified and cloned into *E. coli* expression vectors in prior work (Bonander & Cornell, 2007; Ormond, Simkin, & Cornell, 2007). Briefly, gene specific PCR primers were used to amplify the target genes and clone them into pTrcHis-TOPO[®] plasmid vectors (Invitrogen) to create chimeras encoding hexahistidine sequences fused to the C-terminus of the MTN enzymes. The plasmids were transformed and expressed in *E. coli* BL21 (DE3) pLysS cells maintained on Luria Bertani (LB) agar supplemented with 100µg/mL ampicillin. The clone for *E. coli* MTN was maintained and expressed as previously reported (Cornell & Riscoe, 1998; Lee, Cornell, Riscoe, & Howell, 2001). A plasmid clone for hexahistidine tagged human MTAP (kind gift of Dr. V. Schramm, Albert Einstein) was similarly transformed into *E. coli* BL21 (DE3) pLysS cells.

Recombinant enzymes were expressed as previously described (Cornell & Riscoe, 1998). Briefly, isolated bacterial colonies were used to inoculate a 10 mL culture of LB broth supplemented with 100µg/mL ampicillin (LBamp¹⁰⁰) and grown overnight at 37° C with shaking. Induction cultures were initiated by diluting the overnight culture into 500 mL of fresh LBamp¹⁰⁰ broth and incubating at 37° C with shaking (225 RPM) until the optical density of the culture at 600 nm (OD₆₀₀) reached 0.5. Recombinant protein expression was induced by addition of isopropylthiogalactoside (IPTG) to 1.0 mM final concentration. Cultures were induced overnight at 30° C. Cells were harvested via

centrifugation at 4000 xg for 10 min. The bacterial cell pellet was washed in sterile PBS and re-centrifuged at 4000 xg. Cells were lysed using either sonication or B-PER™ reagent (Pierce, Rockford, IL) and centrifuged at 12,000 xg for 15 min to remove debris.

Recombinant proteins were purified from the clarified lysate by cobalt affinity chromatography using His-Pur Cobalt™ resin according to the manufacturer's specifications (Pierce, Rockford, IL). Briefly, the clarified lysate was mixed with an equal volume of His-Pur Cobalt™ resin and rocked overnight at 4° C to bind the recombinant enzymes. The resin was recovered by centrifugation at 700 xg for 2 min at 4° C to remove unbound material. The resin was sequentially washed with two 6 ml volumes of 1 mM imidazole buffer (pH 7.2), and one 6 mL volume of 20 mM imidazole buffer (pH 8) to remove weakly bound protein. Recombinant hexahistidine-tagged MTN and MTAP enzymes were specifically eluted with three 3 mL volumes of 500 mM imidazole (pH 8.0). Residual protein was stripped from the resin using one 3 mL elution with 1 M imidazole (pH 8.0). Protein concentrations in fractions were estimated using a Bio-Rad microassay (Bio-Rad, Hercules, CA) modification of the Bradford assay (Bradford, 1976). Glycerol was added to enzyme containing fractions to a final concentration of 20%, and the fractions stored -80 °C.

Analysis of MTN and MTAP Proteins

Affinity purified MTN and MTAP enzymes (5-10 µg) were analyzed for homogeneity on 12% acrylamide SDS-PAGE gels electrophoresed at 66 mA for 45 minutes. Proteins were visualized by Coomassie Brilliant Blue staining (0.1% Coomassie Brilliant Blue in 50% methanol/10% glacial acetic acid). Molecular weight was confirmed by comparison to an EZ-Run Pre-stained Rec Protein standard (Thermo

Fisher Scientific, Rockford, IL). Gel images were collected using a ProteinSimple FluorChem E imager.

Determination of Protein Concentration

The concentration of purified proteins were determined by UV spectrophotometry at 280 nm using a Varian Cary 50 spectrophotometer and the application of Beer's law, $A = \epsilon lc$ (Simonian, 2004). The extinction coefficients at 280 nm (ϵ_{280}) were determined using the ExPASy ProtParam tool (www.expasy.org), and were as follows: EH MTN 0.592 mg/ml⁻¹cm⁻¹, GI MTN-10.618 mg/ml⁻¹cm⁻¹, GI MTN-2 0.404 mg/ml⁻¹cm⁻¹, and human MTAP 0.959 mg/ml⁻¹cm⁻¹.

MTN Activity: Enzyme Assays

The specific activity of purified MTN and MTAP enzymes was determined by monitoring the loss of absorbance at 275 nm ($\epsilon_{275} = 1.6 \text{ mM}^{-1} \text{ cm}^{-1}$) that occurs when MTA is cleaved into MTR and adenine (Singh, Evans, et al., 2005). Enzyme reactions contained 0.1 M potassium phosphate buffer (pH 7) and 100 μM MTA with a total volume of 990 μl . The assay was initiated by addition of enzyme (1-4 μg) in 10 μL and rapid mixing. A Varian Cary 50 spectrophotometer was used to measure absorbance changes at 275 nm and the specific activities calculated in U/mg (1 U = 1 $\mu\text{mol}/\text{min}$ MTA conversion). Enzyme kinetics assays were similarly performed using varying substrate (MTA, SAH, 5'dADO) concentrations (1 – 100 μM). Results were plotted on [S] vs. V graphs, and kinetic constants (K_m , k_{cat}) determined by fitting the data to the Michaelis-Menten equation (Eq. 1) using GraphPad Prism (GraphPad Software, Inc., La Jolla, CA).

(Equation 1)
$$V_o = \frac{V_{max}[S]}{K_m + [S]}$$

MTN Inhibition Assay

Initial *in-silico* computational screening by Dr. Danny Xu (Idaho State University, Meridian, ID) identified 33 potential competitive inhibitors of MTN based on screening of the National Cancer Institute (NCI) diversity set II compound database (~4200 compounds) against known crystal structures for the *E. coli* MTN. The 33 potential inhibitors were obtained from the NCI and analyzed for *in vitro* anti-MTN activity using the UV spectrophotometric assay (275 nm) described above. In the assay, MTA substrate concentrations (20 – 200 μM) and inhibitor concentrations (0 – 100 μM) were used. Inhibitor constants were determined by two methods. In the first method, velocity measurements were collected at a constant substrate concentration with varying inhibitor concentrations (Singh, Evans, et al., 2005). The ratio of inhibited to uninhibited velocity (V_o'/V_o) was plotted as a function of inhibitor concentration. Inhibitor constants (K_i 's) were obtained by fitting the results to the equation for competitive inhibition (Eqn. 2).

$$\text{(Equation 2)} \quad V_o'/V_o = (K_m + [S]) / \{(K_m + [S]) + (K_m[I]/K_i)\}$$

In the second method, several inhibitor concentrations were tested for effects against increasing substrate concentrations. The resulting substrate-velocity data was fit to equations for competitive (Eq. 3), uncompetitive (Eq. 4), and mixed inhibition (Eq. 5) using GraphPad Prism. The “best fit” was assigned based on r^2 values.

$$\text{(Equation 3)} \quad V_o = (V_{\max} [S]) / \{K_m (1 + [I]/K_i) + [S]\}$$

$$\text{(Equation 4)} \quad V_o = (V_{\max} [S]) / \{K_m + [S](1 + [I]/K_i)\}$$

$$\text{(Equation 5)} \quad V_o = (V_{\max} [S]) / \{K_m (1 + [I]/K_i) + [S](1 + [I]/K_i)\}$$

Cell Growth Assays

Giardia intestinalis Resazurin Reduction Assay

Giardia intestinalis (clone WB C6) cells were grown at 37 °C in sealed T-25 flasks containing in sterile TYDK media (Valdez et al., 2009) supplemented with adult bovine serum (Thermo Scientific), Ox bile (MP Biomedicals, Solon, OH), Fungizone (Omega Scientific Inc., Tarzana, CA), and Pen-Strep (Thermo Scientific). To prepare cultures for antibiotic tests, cells were harvested from near-confluent culture by placing on ice up to one hour promote cell detachment. The detached-cell sample was split between two 50 ml conical tubes and centrifuged at 500 xg for 5 minutes to pellet the cells. The supernatant was then decanted and cells were re-suspended into 5 mL of fresh TYDK broth. The cell concentration and viability was determined using a hemacytometer and Trypan blue staining (Sigma), and the cell suspension volume adjusted with TYDK broth to obtain a concentration of 1×10^6 trophozoites/ml.

Antibiotic activity studies were conducted in 96 well plates containing drug (0 – 100 μ M), TYDK broth, and 1×10^4 *Giardia* trophozoites in a final volume of 300 μ L. The standard anti-giardial agent metronidazole (MTZ) served as a control in drug sensitivity studies. Plates were sealed with thin film and incubated in anaerobic chambers at 37 °C for 64 hours. The media in the wells was then replaced with 300 μ l of 0.1% resazurin (MP Biomedicals) in PBS supplemented with 0.1% glucose. Fluorescence measurements were made using on a BioTek Synergy HT plate reader (Em. 530 nm/Ex. 590 nm), and the plates returned to the anaerobic chamber. Additional fluorescence readings were conducted at 68 and 72 hr.

Giardia intestinalis BacTiter-Glo™ Assay

Additional drug sensitivity studies were conducted as previously described (Debnath et al., 2012; Tejman-Yarden et al., 2013). In brief, sterile opaque-walled 96 well plates were assembled containing *Giardia intestinalis* cells (10^4 trophozoites/well) and drug (0-100 μ M) in a final volume of 100 μ L TYDK media. Metronidazole treatment (0-100 μ M) served as a control. Plates were placed in an anaerobic chamber and incubated at 37° C for 72 hrs. Cell proliferation was measured by assessing ATP content by the addition of 100 μ L BacTiter-Glo™ reagent (Promega, Madison, WI) to each well. Luminescence was recorded for five minutes using a BioTec Synergy HT plate reader.

Mammalian Cell Line Resazurin Reduction Assays

Hela cells were cultured at 37° C in a 5% CO₂ humidified atmosphere using Dulbeccos Modified Eagles Medium (DMEM) supplemented with 10% FBS and Pen-Strep. Cells were harvested by brief treatment with Trypsin-EDTA (MP Biomedicals), dilution of detached cells with 10 mL DMEM, and centrifugation at 250 xg for 5 minutes. The cell pellet was resuspended in 10 mL fresh DMEM and the viability and density determined by Trypan blue staining and hemacytometry. Cells were diluted to a final concentration of 25,000 cells/mL, and 200 μ l of cells and media were pipetted into each well of a sterile 96 well plate. Plates were incubated at 37 °C for 24 hr in a 5% CO₂ humidified atmosphere. After 24 hr, media was replaced with 200 μ l of fresh media containing 0-100 μ M drug. Plates were cultured for an added 48 hr, at which time 20 μ l of 0.1% resazurin in 1X PBS was added to each well, and the plates re-incubated for

another 24 hrs. At 72 hr, fluorescence (Ex. 485 nm/Em. 528 nm) was measured using a BioTek Synergy HT plate reader.

Jurkat cells were cultured at 37° C in a 5% CO₂ humidified atmosphere using RPMI 1640 media supplemented with 10% FBS and Pen-Strep. Cells were harvested by centrifugation and the cell pellet resuspended in media to a final concentration of 5.5 x 10⁴ cells/mL. Drug sensitivity plates contained 0-100 μM drug and 1 x 10⁴ Jurkat cells/well in a final volume of 200 μL. At 48 hr, 20 μl of 0.1% resazurin in 1X PBS was added to each well. At 72 hr, fluorescence measurements (Ex. 485 nm/Em. 528 nm) were made using a BioTek Synergy HT plate reader.

CHAPTER THREE: RESULTS AND DISCUSSION

Purity and Activity of Proteins

Milligram quantities of overexpressed recombinant enzymes were purified by cobalt affinity chromatography. Protein purity was confirmed by SDS PAGE (Figure 13). All the enzymes showed > 95% purity. The molecular weights for *Entamoeba* MTN (EH, 29,434 D), *Giardia* MTN-1 (33,034 D), and MTN-2 (35,773 D) calculated from the molecular weights of enzyme monomers fused to the affinity sequences derived from the pTrcHis-TOPO[®] vector using the ExPASy ProtParam tool (www.expasy.org)

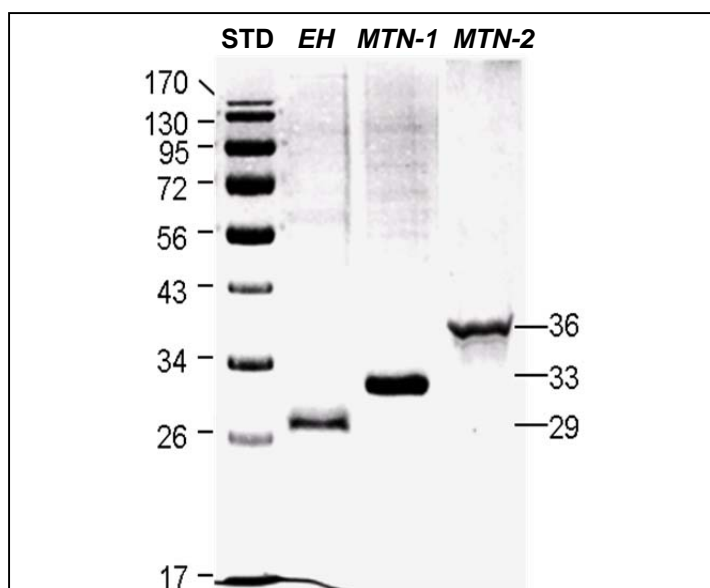


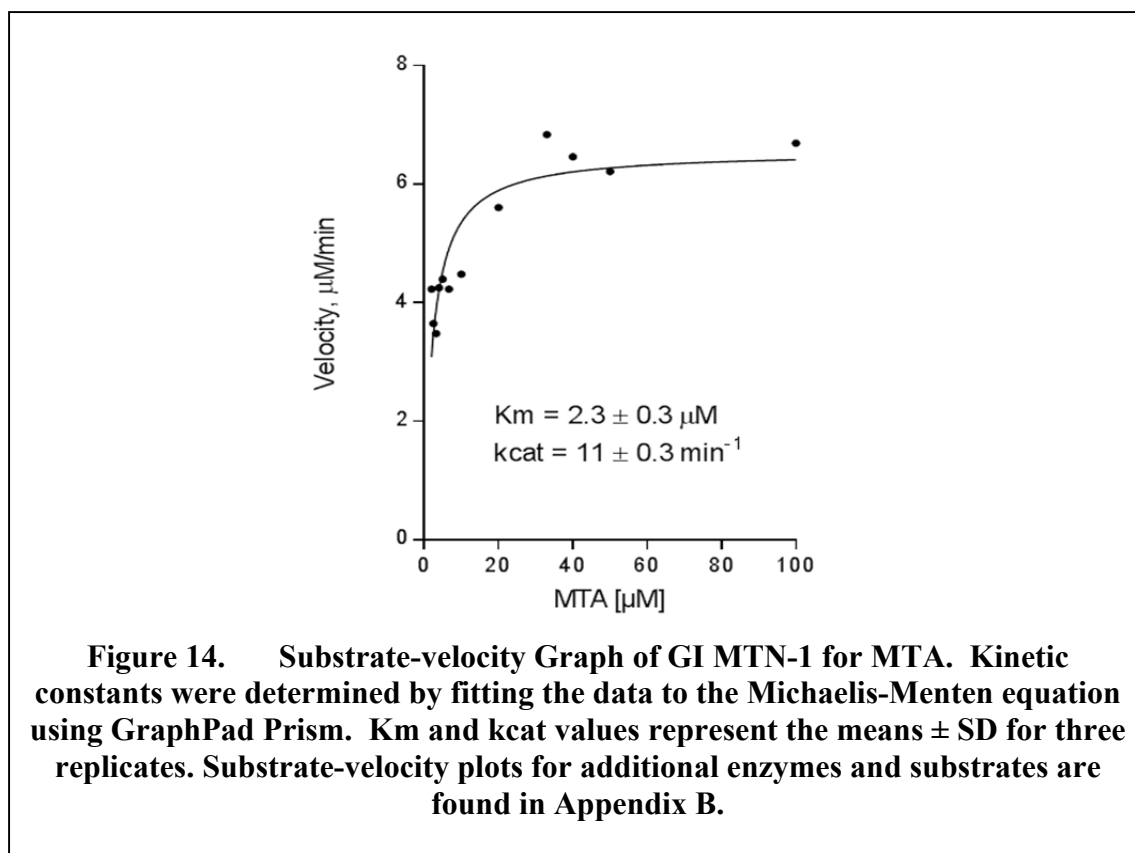
Figure 13. SDS-PAGE of Recombinant Proteins. Cobalt affinity purified enzymes were electrophoresed on a 12% polyacrylamide gel. All three enzymes showed greater than 95% purity. Estimated molecular weights for the enzymes were 29 kD (EH), 33 kD (GI MTN-1) and 36 kD (GI MTN-2).

were consistent with the apparent molecular weights estimated from the gel.

Previous specific activity measurements performed at saturating concentrations of MTA, 5'dADO, and SAH substrates demonstrated that both MTA and 5'dADO were substrates for all three parasite enzymes (Bonander & Cornell, 2007; Ormond, et al., 2007; Stone, Eidemiller, & Cornell, 2012). SAH was not a substrate for EH MTN and GI MTN-1, but was a substrate for GI MTN-2 (Stone et al., 2012). EH, GI MTN-1, and GI MTN-2 showed specific activities for MTA of 11.0, 0.3, and 0.2 U/mg (1 U = 1 μ mol/min), respectively, and 5.0, 0.3, and 0.2 U/mg for 5'dADO. These specific activities are lower than those reported for the bacterial *E. coli* MTN (4.4 U/mg) or *B. burgdorferi* MTN (4.1 U/mg) (Cornell, Swarts, Barry, & Riscoe, 1996; Cornell, et al., 2009). However, it is in good agreement with data collected previously on EH and GI MTN-1 proteins purified previously in the Cornell lab that showed specific activities for MTA of 11.5 and 0.37 U/mg, respectively, and 5.9 and 0.24 U/mg, respectively, against 5'-dADO (Hall, Martinez, & Cornell, 2012). It appears that the eukaryotic MTNs display less activity overall. Consistent with this observation, the MTN of the tomato fruit (*Lycopersicon esculentum*) appear to show a maximum activity of only 0.0012 U/mg protein, though this protein was purified from native sources and was not a pure recombinant source (Kushad, Richardson & Ferro, 1985).

To prepare for later inhibition studies, the kinetic constants for MTA and 5'dADO were determined for the three parasite enzymes. A representative substrate-velocity graph for the activity of GI MTN-1 is presented in Figure 14. Additional substrate-velocity graphs are presented in Appendix B. The results of kinetic analyses for the three parasite enzymes and *E. coli* MTN are summarized in Table 2. In general, the parasite enzymes

demonstrated K_m values for MTA in the 2 – 5 μM range, approximately an order of magnitude larger than the K_m for MTA found for the *E. coli* enzyme (0.5 μM). In *Arabidopsis* MTNs, K_m values reported for MTA were both above 20 μM , while in *Lupines luteus* seeds the K_m value reported for MTA was only 0.41 μM (Park et al., 2009; Guranowski, Ghiang, & Cantoni, 1981). However, other authors have reported K_m values for MTA of 2.1 μM in *Oryza* (rice) and 3.4 -7.1 μM in *Arabidopsis*, which are similar to the K_m values reported here for the parasite enzymes (Rzewuski et al., 2007; Siu et al., 2008). A K_m value of 8.7 μM for MTA was also reported for the MTA/SAH nucleosidase of *Klebsiella pneumonia* that shares closer homology to the proteins studied here (Cornell, Winter, Tower, & Riscoe, 1996). Overall, it is important to note that, just as was reported to be the case in *Burkholderia thailandensis*, these enzymes all share one common trait, they have a greater specificity for MTA than for the other possible substrates (Gao, Zheng, & Yuan, 2013).



As seen in Table 2, the *E. coli* MTN also showed greater catalytic efficiency for the substrates than the parasite enzymes. Generally, the catalytic efficiencies (k_{cat}/K_m) were best for the MTA substrate, indicating that it is the preferred substrate of the parasite enzymes.

Table 2 Summary of Recombinant Parasite MTN Substrate Kinetics

Enzyme	Substrate	K_m (μM)	k_{cat} (s^{-1})	k_{cat}/K_m ($\text{s}^{-1}\mu\text{M}^{-1}$)
<i>E. coli</i> MTN	MTA	0.5 ± 0.2	1.7 ± 0.1	3.4 ± 0.5
	5'dAdo	0.8 ± 0.2	3.0 ± 0.1	3.6 ± 0.7
	SAH	1.3 ± 0.2	2.6 ± 0.1	2.1 ± 0.3
<i>EH</i> MTN	MTA	4.5 ± 0.4	5.3 ± 0.1	1.2 ± 0.3
	5'dAdo	3.8 ± 0.7	2.4 ± 0.1	0.6 ± 0.1
	SAH	NA	NA	NA
<i>GI</i> MTN-1	MTA	2.3 ± 0.3	0.2 ± 0.01	0.09 ± 0.03
	5'dAdo	9.8 ± 1.5	0.2 ± 0.01	0.02 ± 0.001
	SAH	NA	NA	NA
<i>GI</i> MTN-2	MTA	5.3 ± 1.0	0.1 ± 0.01	0.02 ± 0.006
	5'dAdo	10.7 ± 1.7	0.1 ± 0.01	0.01 ± 0.006

A k_{cat}/K_m ratio of *EH* MTN was calculated as $1.2 \text{ s}^{-1}\mu\text{M}^{-1}$ for MTA and $0.6 \text{ s}^{-1}\mu\text{M}^{-1}$ for 5'dAdo, only half the value for MTA. The efficiency of *GI* MTN-1 was $0.09 \text{ s}^{-1}\mu\text{M}^{-1}$ for MTA and $0.02 \text{ s}^{-1}\mu\text{M}^{-1}$ for 5'dAdo, less than a third the value of MTA. The efficiency of *GI* MTN-2 was $0.02 \text{ s}^{-1}\mu\text{M}^{-1}$ for MTA and $0.01 \text{ s}^{-1}\mu\text{M}^{-1}$ for 5'dAdo. These numbers suggest a much higher efficiency of *EH* MTN compared to either of the *Giardia* MTNs although the efficiency for MTA as a substrate is always the highest for all three enzymes. The comparatively more active *E. coli* MTN, with a $3.4 \text{ s}^{-1}\mu\text{M}^{-1}$ efficiency for MTA, can possibly be explained by a lack of an SAHH in its genome and also a lack of other MTN proteins capable of catabolizing all of the substrates that build up inside the cell. *E. histolytica* has an SAHH in its genome that would reduce the necessity for a very active MTN enzyme. Interestingly, the plant *Arabidopsis thaliana* genome encodes two MTNs and a SAHH, and the MTNs show efficiencies of $0.6\text{-}2.6 \text{ s}^{-1}\mu\text{M}^{-1}$ for MTA (Siu et al., 2008). This is similar to the values reported here for the *Entamoeba* enzyme. Similar to *Arabidopsis*, *G. intestinalis* encodes two MTNs. However, *Giardia* lacks an SAHH,

and the efficiencies for MTA and 5' dAdo are lower than the other reported enzymes. This suggests that the organism may use its MTNs to hydrolyze a variety of nucleosides to supply purines for the cell, and thus the MTNs have low efficiency for any one substrate. Or, the enzyme conditions for optimal activity have yet to be achieved. To date, ten complete *Giardia* genome sequences have been submitted to the Uniprot database, and all have contained two putative MTN genes. This may further support the idea that the activity of each enzyme is of less importance than the combined activity of both of the MTN enzymes.

MTN Inhibition Assays

The initial 33 compound hits from the *in-silico* screening (against *E. coli* MTN) were tested by UV spectrophotometric assay for inhibitory activity against the *E. coli* MTN. This resulted in the identification of four compounds with measurable inhibitory activity (listed in Table 3). These four compounds were expected to be good inhibitors against both the *Giardia* and *Entamoeba* MTNs because of the overall high homologies in MTN active sites. Initial tests using equal concentrations of MTA substrate and drug showed definite inhibition of parasite MTN activity.

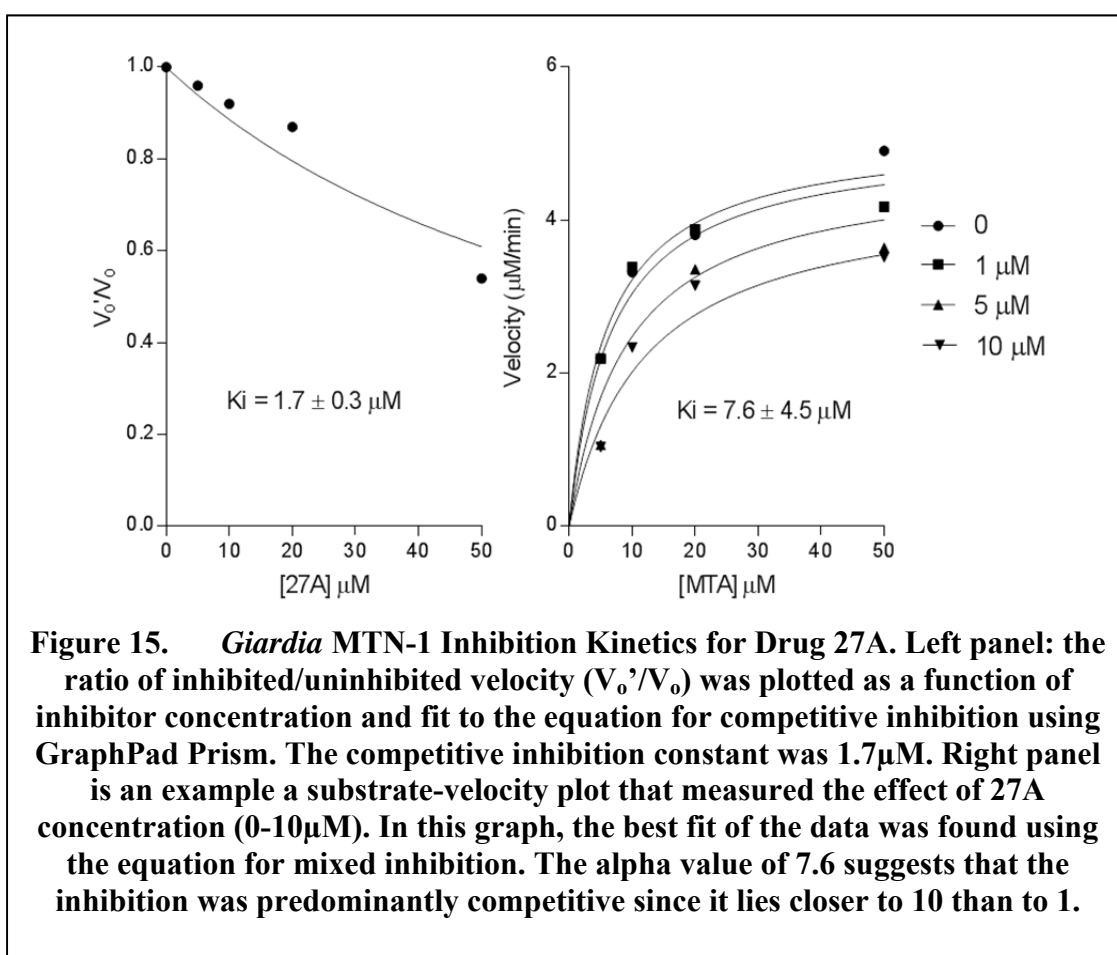
Table 3 IUPAC Names of MTN Inhibitors	
Drug	IUPAC Name
5A	N-(2-furylmethyl)-N'-(4-nitrophenyl)urea
8A	1-(4-nitrophenyl)-3-[4-[4[(4-nitrophenyl) carbamoylamimino] phenoxy]phenyl]-urea
15A	2-[2-(5,6-dimethyl-1H-benzoimidazol-2-yl)viny]l]-5,6-dimethyl-1H-benzoimidazole
27A	3-(1,3-benzothiazol-2-yl)-1-(5-[(1,3-benzothiazol-2-yl)carbamoyl]amino)-2-methylphenyl)urea

Inhibitor constants were determined for the four compounds using the method of Singh, Evans, et al. (2005) that measures the ratio of the inhibited initial velocity to the

uninhibited velocity as a function of the inhibitor concentration (Figure 15, left panel).

The results were fit to the Michaelis-Menten equation for competitive inhibition (Eqn. 2).

This method works well with high affinity competitive inhibitors, but is not readily useful for inhibitors that bind by mixed or uncompetitive modes. Since the drugs were initially identified by *in-silico* calculations of their capacity to bind the active site of the enzymes, it is reasonable to assume that the primary mode of inhibition would be competitive, and this generally is what was seen (Figure 16).



To determine if other modes of inhibition were occurring, and to attempt to find K_i values for data that failed to readily fit the approach used by Singh, Evans, et al., inhibition constants were also determined by measuring the effect of varied

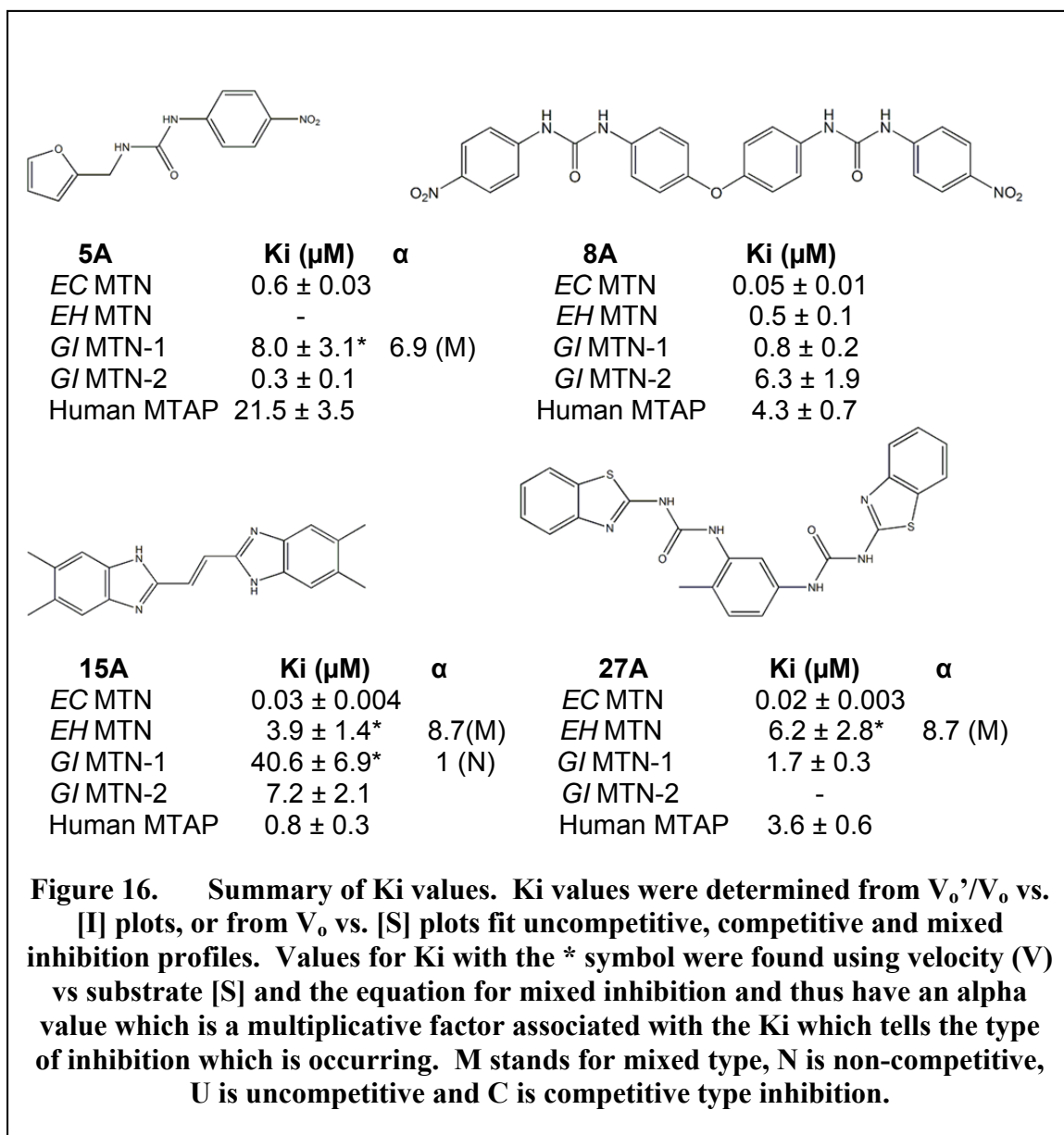
concentrations of inhibitor (1-20 μM) across a range of substrate concentrations (1-50 μM). The results were presented as substrate (S) vs velocity (V) plots, and the data fit to the Michaelis-Menten equation for competitive, uncompetitive, and mixed inhibition (Eqs. 3-5) using GraphPad Prism. As can be seen in Figure 15 (right panel), the best fit for drug 27A inhibition was obtained using the model for a mixed inhibitor. The alpha value (7.6) indicates that competitive inhibition was the predominant contributor to the mixed inhibition profile produced by drug 27A.

The software reported an alpha value that helped to determine the mode of inhibition of each drug against each enzyme. If the alpha value, which can be seen in Equation 6, was less than 1 then the mode was uncompetitive, when it is 1 then it is noncompetitive, when it is greater than one but less than 10 then there is a mix of uncompetitive and competitive, and if it is larger than 10 then the mode matches the competitive model (GraphPad Prism User's Manual).

$$\text{(Equation 6)} \quad V = \frac{(v_{max})[S]}{\left(Km\left(1+\frac{[I]}{Ki}\right)\right) + \left([S]\left(1+\frac{[I]}{\alpha Ki}\right)\right)}$$

Compounds that inhibited the reaction the strongest showed the lowest K_i values. When tested against *E. coli* MTN, compounds 5A, 8A, 15A, and 27A yielded K_i values of 0.6, 0.05, 0.03, and 0.02 μM , respectively. All were competitive inhibitors of the *E. coli* enzyme (Figure 16). These values are three to six orders of magnitude higher than the K_i values of the nucleoside transition state analogs of MTA reported for *E. coli* MTN (Singh et al., 2004; Singh, Evans, et al., 2005; Gutierrez et al., 2007). However, transition state analogues have nearly perfect structure and electrostatics, which allow for extremely tight binding (Lee et al., 2005). However, the purpose of looking at compounds identified by *in-silico* screening (rather than transition state analogs), is that

they are novel drug leads that do not resemble the substrates. Thus, they may show more effective transport properties and more discrimination for pathogen MTNs. These compounds will serve as lead scaffolds for further optimization studies.



When tested against the parasite MTNs, the inhibitors mostly displayed high nanomolar to low micromolar inhibition constants. Compound 5A failed to inhibit the *Entamoeba* MTN, but showed a 0.3 μM competitive inhibition constant for *Giardia*

MTN-2 and mixed inhibition against MTN-1. Overall, compound 8A showed some of the most potent inhibition profiles for the parasite enzymes. Compound 8A showed strict competitive inhibition with 0.5-0.8 μM inhibition constants against *Entamoeba* and *Giardia* enzymes. While compounds 15A and 27A showed the tightest binding to *E. coli* MTN, their binding profiles were the weakest to the parasite MTNs.

An indication of drug specificity for target MTNs was gained by examining inhibition profiles against human MTAP, as has been previously reported for transition state analogs of MTA (Longshaw et al., 2010). This difference suggests that use of these drugs against a target organism will not cause serious side effects in the host. It is also unlikely that drug inhibition of MTAP by a drug used only in the short term would cause any permanent harm to the human host. In addition, transition state analogs that were found to be more potent against MTAP rather than target MTNs may make attractive anti-cancer agents, although that is beyond the scope of this thesis (Clinch et al., 2012; Singh et al., 2004). The initial *in vitro* testing showed that most of the compound K_i values were higher for human MTAP than seen for the microbial MTNs. The exceptions were 15A and 27A, which showed tighter binding to the human MTAP than most of the parasite MTNs.

Table 4 summarizes the K_i discrimination factors found for the four inhibitors. These discrimination factors were obtained by dividing the MTAP drug K_i by the MTN drug K_i values (Longshaw et al., 2010). Larger discrimination factors are desirable, since they indicate more specificity for the target MTNs. All four compounds showed high K_i discrimination factors (35.8 to 157.0-fold) for the *E. coli* MTN compared to human MTAP. However, for the parasite MTNs, only compound 5A showed a high

discrimination factor (65.1-fold) for GI MTN-2 compared to MTAP. The other discrimination factors were either modest, or showed a preference for human MTAP. The development of larger discrimination factors will be a primary goal of drug optimization.

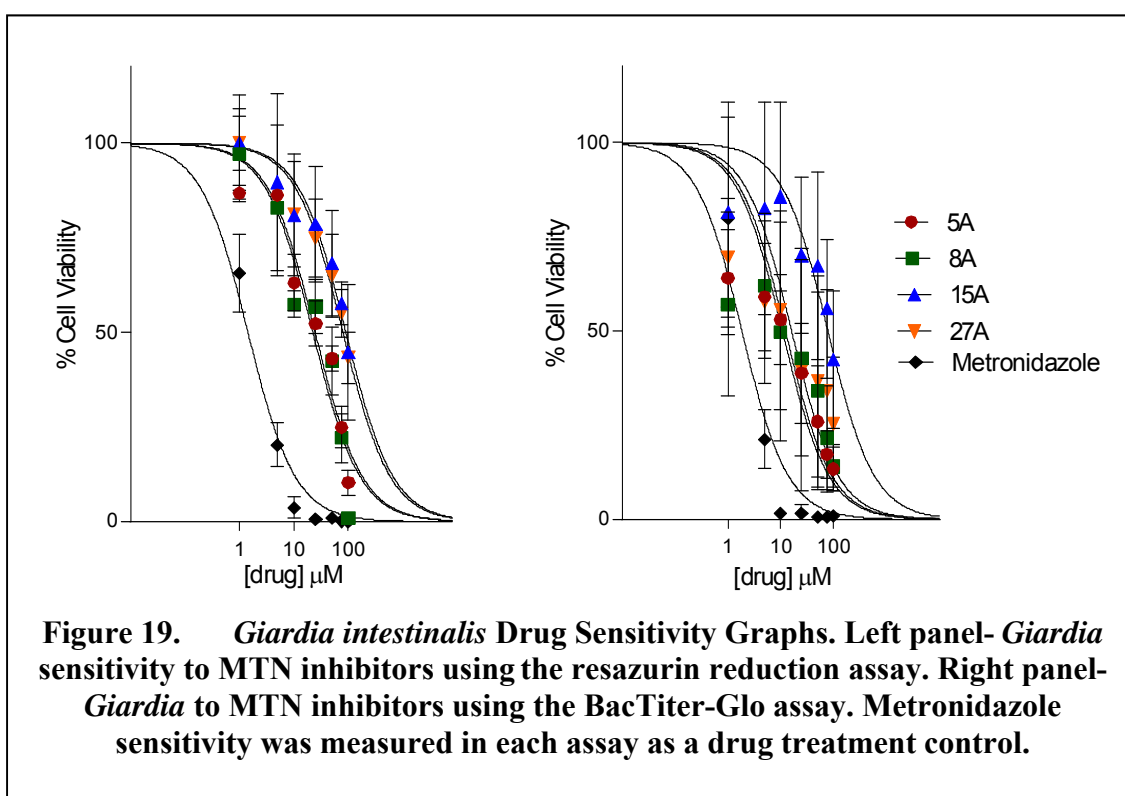
Drug	Ki MTAP/ Ki E.coli MTN	Ki MTAP/ Ki EH MTN	Ki MTAP/ Ki GI MTN-1	Ki MTAP/ Ki GIMTN-2
5A	35.8	NA	6.1*	65.1
8A	79.3	8.4	5.3	0.7
15A	25.3	0.2*	0.2*	0.1
27A	157.0	0.9*	2.1	NA

NA means a Ki value could not be determined. * indicates discrimination factors determined using mixed inhibition Ki values for the MTN.

***Giardia intestinalis* Drug Sensitivity**

The ability of MTN inhibitors to exert antiproliferative effects against *Giardia intestinalis* trophozoites (WB clone G6) was examined using a resazurin reduction assay (Nillius, Müller, & Müller, 2011; Bénéré, de Luz, Vermeersch, Cos, & Maes, 2007) that follows the conversion of resazurin to fluorescent resorufin in viable cells (Figure 17). In this assay, the fluorescence signal strength can be correlated to viable cell number and used to estimate drug IC₅₀ values. Unfortunately, this test is susceptible to media interferences. TYDK media used to grow *Giardia* causes nonspecific reduction of resazurin, resulting in elevated background signals that limit assay sensitivity. To bypass this effect, the media in the assay is replaced with PBS-glucose containing the resazurin dye. However, this adds to the labor involved in the assay and potentially introduces error to the experiment.

IC₅₀ values of 24.5 and 22.2 μM, respectively (Table 5). Since both of these compounds also exerted submicromolar K_i values for at least one of the *Giardia* MTNs, these two seem to be the most desirable of the four compounds to further develop. The compounds 15A and 27A also killed *Giardia*, but with IC₅₀ values of 80-90 μM. These compounds could still be viable candidates for use as anti-parasitics after more optimization. The results seem to roughly correlate with the *in vitro* K_i values, which suggested that 5A and 8A are better inhibitors of *Giardia* MTN than are drugs 15A and 27A.



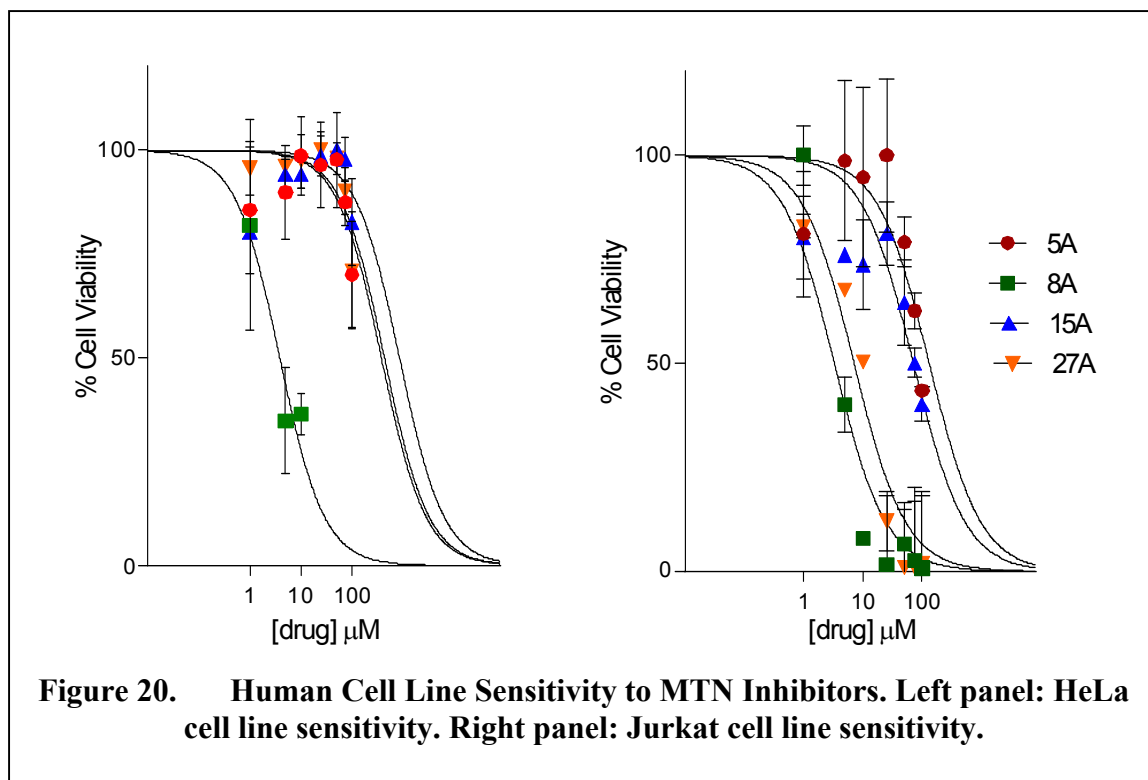
The IC₅₀ concentrations found using the BacTiter-Glo™ method (Figure 19, left panel; Table 5) were consistently lower than those found using the resazurin reduction assay. Drug 5A (IC₅₀ = 10.8 μM) actually outperformed any of the other drugs in this assay, with the exception of the metronidazole (IC₅₀ = 1.9 μM). Drugs 8A and 27A were slightly less potent, with IC₅₀s of 12.3 and 16.12 μM, respectively. The weakest inhibitor

was 15A with an IC_{50} of 78.9 μ M. These results suggest that the enzyme K_i values were fairly good predictors of anti-giardial activity: tighter binding drugs (lower K_i 's) showed more potent activity *in vitro* against parasite cultures.

None of the compounds were as potent as metronidazole ($IC_{50} = 1.4-1.9 \mu$ M), or the recently reported Auranofin ($IC_{50} = 4-6 \mu$ M) (Tejman-Yarden et al., 2013). However, the MTN inhibitors are intended as lead compounds that will be further optimized via derivatization of the compound to lower their IC_{50} values and improved their discrimination for parasite MTNs. In this regard, the testing of putative MTN inhibitors identified by *in-silico* screening has been a success. Several compounds, 5A in particular, showed the ability to discriminate between the parasite and human enzymes, and showed *in vitro* activity against parasite cultures.

Human Cell Line Drug Sensitivity

The drug leads were reasonably non-toxic to HeLa cell cultures, with the exception of drug 8A, which showed an IC_{50} value of 6.2 μ M (Figure 20, left panel; Table 5). The other drugs (5A, 15A, 27A) showed IC_{50} values in excess of 400 μ M, dramatically higher than their corresponding IC_{50} s for parasite cultures (Table 5). These results suggest that 8A would not make a great anti-parasitic without optimization, but instead may make an attractive anti-cancer agent. It is interesting to note that drug 8A actually had one of the higher K_i values against human MTAP in the *in vitro* enzyme activity tests. This may indicate that there is some other mechanism of action that is causing the drug to be lethal to the HeLa cells other than strict inhibition of MTAP.



The results from that analysis of anti-proliferative effects on Jurkat cells pose more of a problem for the drugs as possible anti-parasitic candidates. While the general pattern found in the HeLa cells seems to be repeated, the one notable exception is that drug 27A appears to kill Jurkat cells almost as well as drug 8A. The 8A IC_{50} for Jurkat cells is 3.3 μM , well below the 12-22 μM IC_{50} for *Giardia*. Drug 27A follows close behind with an IC_{50} of 7.1 μM . Again, drug 5A appears to be most promising, with an IC_{50} of 131.9 μM against Jurkat cells, well above the IC_{50} shown for *Giardia*. 15A seem to have about the same IC_{50} level for Jurkat cells as they did for *Giardia*, 71.4 μM and 90.1 μM , respectively. It is important to note that Jurkat cells are a highly proliferative cell line, which may mean that they are more reliant on MTAP for purine and methionine salvage than other cells, and are thus more sensitive to the MTN inhibitors studied here.

Table 5 Summary of Drug IC₅₀ Values (in μM)

	Inhibitor IC ₅₀ ($\mu\text{M} \pm \text{SEM}$)				
	5A	8A	15A	27A	MTZ
<i>Giardia</i>	24.5 \pm 1.7 ¹	22.2 \pm 1.5 ¹	90.1 \pm 1.4 ¹	79.7 \pm 1.5 ¹	1.4 \pm 1.6 ¹
	10.8 \pm 1.4 ²	12.3 \pm 1.2 ²	78.9 \pm 1.2 ²	16.2 \pm 1.2 ²	1.9 \pm 1.3 ²
Hela	421.1 \pm 1.1	6.2 \pm 0.9	868.2 \pm 1.0	438.7 \pm 1.3	NA
Jurkat	131.9 \pm 1.3	3.3 \pm 1.3	71.4 \pm 1.3	7.1 \pm 1.4	NA

¹Results from resazurin reduction assay (Nillius et al., 2011; Bénéré et al., 2007).

²Results BacTiter-Glo™ assay (Valdez et al., 2009). NA means not applicable. Values represent the average of at least three experiments \pm SEM.

CHAPTER FOUR: CONCLUSION

The emergence of drug resistance in parasitic protozoa, and the likelihood of continued expansion of that resistance to other parasites, is a cause of major concern to health authorities. This alarming situation creates a need to develop novel anti-parasitic agents. Promising drug leads have been found through *in-silico* computational drug screening methods. These drug leads appear to target the parasitic forms of the MTN enzyme with high binding affinities while binding the human correlate enzyme MTAP with a lesser affinity as was predicted by the computer simulations. A positive association was found between MTN inhibition and drug IC_{50} values against the target organism, *Giardia intestinalis*. This suggests that the drug activity is due to the inhibition of the parasitic MTN and not due to other possible off-target effects of the drugs. This study has proved that *in-silico* methods can be employed to discover novel drug leads that are effective against parasitic protozoan MTNs and serves to promote further *in-silico* studies against other organisms that require MTN activity to salvage methionine and purines from nucleoside by-products of SAM mediated reactions in the cell.

REFERENCES

- Abboud P, Lemée V, Gargala G, Brasseur P, Ballet JJ, Borsa-Lebas F, Caron F, Favennec L. Successful treatment of metronidazole- and albendazole-resistant giardiasis with nitazoxanide in a patient with acquired immunodeficiency syndrome. *Clin Infect Dis* **2001**, 32 (12), 1792-4.
- Alekshun MN; Levy, SB. Molecular mechanisms of antibacterial multidrug resistance. *Cell* **2007**, 128 (6), 1037-50.
- Ali SA; Hill DR. *Giardia intestinalis*. *Curr Opin Infect Dis*. **2003**, 16(5), 453-60.
- Alkire S, JR, Seth S. *Multidimensional Poverty Index*; University of Oxford: Oxford England, **2013**.
- Anderson AC. The Process of Structure-Based Design. *Chemistry and Biology* **2003**, 10, 787-797.
- Auerbach PS. *Wilderness medicine*. 6th ed.; Mosby Elsevier: Philadelphia, **2007**.
- Bansal D, Malla N, Mahajan RC. Drug resistance in amoebiasis. *Indian J Med Res*. **2006**, 123, 115-118.
- Bénére E, da Luz RA, Vermeersch M, Cos P, Maes L. A new quantitative in vitro microculture method for *Giardia duodenalis* trophozoites. *J Microbiol Methods* **2007**, 71 (2), 101-6.
- Bonander J, Cornell KA. Purine auxotrophy, *Giardia's* Achilles Heel? Poster Presentation 88th Annual Meeting AAAS Pacific Division June **2007**.
- Bradford MM. A rapid and sensitive method for the quantitation of microgram quantities of protein utilizing the principle of protein-dye binding. *Anal Biochem*. **1976**, 72, 248-54.
- Bush AO, Fernández JC, Esch GW, Seed JR. *Parasitism: The diversity and ecology of animal parasites*. Cambridge University Press: Cambridge, UK, **2001**.
- Cairncross S, Müller R, Zagaria N. Dracunculiasis (Guinea worm disease) and the eradication initiative. *Clin Microbiol Rev* **2002**, 15 (2), 223-46.

CDC. The President's Malaria Initiative. *7th annual report to Congress*, Centers for Disease Control: Washington, D.C., **2013**.

CDC. *Entamoeba* Life Cycle <http://www.dpd.cdc.gov/dpdx> retrieved Feb. **2014 b**.

CDC. *Giardia* Life Cycle <http://www.dpd.cdc.gov/dpdx> retrieved Feb. **2014 a**.

Challand MR, Ziegert T, Douglas P, Wood RJ, Kriek M, Shaw NM, Roach PL. Product inhibition in the radical S-adenosylmethionine family. *FEBS Lett* **2009**, 583 (8), 1358-62.

Chiang PK, Gordon RK, Tal J, Zeng GC, Doctor BP, Pardhasaradhi K, McCann PP. S-Adenosylmethionine and methylation. *FASEB J* **1996**, 10 (4), 471-80.

Clinch K, Evans GB, Fröhlich RF, Gulab SA, Gutierrez JA, Mason JM, Schramm VL, Tyler PC, Woolhouse AD. Transition state analogue inhibitors of human methylthioadenosine phosphorylase and bacterial methylthioadenosine/S-adenosylhomocysteine nucleosidase incorporating acyclic ribooxacarbenium ion mimics. *Bioorg Med Chem* **2012**, 20 (17), 5181-7.

Cornell KA, Primus S, Martinez JA, Parveen N. Assessment of methylthioadenosine/S-adenosylhomocysteine nucleosidases of *Borrelia burgdorferi* as targets for novel antimicrobials using a novel high-throughput method. *J Antimicrob Chemother* **2009**, 63 (6), 1163-72.

Cornell KA, Riscoe MK. Cloning and expression of *Escherichia coli* 5'-methylthioadenosine/S-adenosylhomocysteine nucleosidase: identification of the pfs gene product. *Biochim Biophys Acta* **1998**, 1396 (1), 8-14.

Cornell KA, Swarts WE, Barry RD, Riscoe MK. Characterization of recombinant *Escherichia coli* 5'-methylthioadenosine/S-adenosylhomocysteine nucleosidase: analysis of enzymatic activity and substrate specificity. *Biochem Biophys Res Commun* **1996**, 228 (3), 724-32.

Cornell KA, Winter RW, Tower PA, Riscoe MK. Affinity purification of 5-methylthioribose kinase and 5-methylthioadenosine/S-adenosylhomocysteine nucleosidase from *Klebsiella pneumoniae*. *Biochem. J.* **1996**, 317, 285-290.

Davies J, Davies D. Origins and evolution of antibiotic resistance. *Microbiol Mol Biol Rev* **2010**, 74 (3), 417-33.

Debnath A, Parsonage D, Andrade RM, He C, Cobo ER, Hirata K, Chen S, García-Rivera G, Orozco E, Martínez MB, Gunatilleke SS, Barrios AM, Arkin MR, Poole LB, McKerrow JH, Reed SL. A high-throughput drug screen for *Entamoeba histolytica* identifies a new lead and target. *Nat Med* **2012**, 18 (6), 956-60.

Drisdelle R. *Parasites: tales of humanity's most unwelcome guests*. Berkeley: University of California Press: Berkeley, CA, **2010**.

Durdagi S, Supuran CT, Strom TA, Doostdar N, Kumar MK, Barron AR, Mavromoustakos T, Papadopoulos MG. *In silico* drug screening approach for the design of magic bullets: a successful example with anti-HIV fullerene derivatized amino acids. *J Chem Inf Model* **2009**, *49* (5), 1139-43.

Erickson J, Neidhart D, VanDrie J, Kempf D, Wang X, Norbeck D, Plattener J, Rittenhouse J, Turon M, Wideburg N. Design, activity and 2.8 Å crystal structure of a C2 symmetric inhibitor complexed to HIV-1 protease. *Science* **1990**, (249), 527-533.

Fleming A. *Chemotherapy, Yesterday, To-day and To-morrow*. The Linacre Lecture. London: Cambridge University Press. **1946**.

Fontecave M, Atta M, Mulliez E. S-adenosylmethionine: nothing goes to waste. *Trends Biochem Sci* **2004**, *29* (5), 243-9.

Frey PA, Hegeman AD, Ruzicka FJ. The Radical SAM Superfamily. *Crit Rev Biochem Mol Biol* **2008**, *43* (1), 63-88.

Gao Q, Zheng D, Yuan Z. Substrate preference of 5'-methylthioadenosine/S-adenosylhomocysteine nucleosidase in *Burkholderia thailandensis*. *FEMS Microbiol Lett* **2013**, *339*, 110-116.

Goldberg B, Rattendi D, Lloyd D, Sufrin JR, Bacchi CJ. In situ kinetic characterization of methylthioadenosine transport by the adenosine transporter (P2) of the African *Trypanosoma brucei* and *Trypanosoma brucei rhodesiense*. *Biochem Pharmacol* **2001**, *61*(4), 449-57.

Gopisetty G, Ramachandran K, Singal R. DNA methylations and apoptosis. *Mol Immun* **2005**, *43*, 1729-1740.

Grillo MA, Colombatto S. S-adenosylmethionine and protein methylation. *Amino Acids* **2005**, *28* (4), 357-62.

Guranowski AB, Ghiang PK, Cantoni GL. 5'-Methylthioadenosine nucleosidase purification and characterization of the enzyme from *Lupinus luteus* seeds. *Eur. J. Biochem.* **1981**, *114*, 293-299.

Gutierrez JA, Crowder T, Rinaldo-Matthis A, Ho MC, Almo SC, Schramm VL. Transition state analogs of 5'-methylthioadenosine nucleosidase disrupt quorum sensing. *Nat Chem Biol* **2009**, *5* (4), 251-7.

Gutierrez JA, Luo M, Singh V, Li L, Brown RL, Norris GE, Evans GB, Furneaux RH, Tyler PC, Painter GF, Lenz DH, Schramm VL. Picomolar inhibitors as transition-state probes of 5'-methylthioadenosine nucleosidases. *ACS Chem Biol* **2007**, 2 (11), 725-34.

Hall MP, Ho CK. Characterization of a *Trypanosoma brucei* RNA cap (guanine N-7) methyltransferase. *RNA* **2006**, 12 (3), 488-97.

Hall A, Martinez T, Cornell KA. Characterization of MTA nucleosidases from parasitic protozoa. Poster presentation Idaho INBRE 2012.

Haque R, Mondal D, Duggal P, Kabir M, Roy S, Farr BM, Sack RB, Petri WA. *Entamoeba histolytica* infection in children and protection from subsequent amoebiasis. *Infect Immun* **2006**, 74 (2), 904-9.

Hajduk PJ, Greer J. A decade of fragment-based drug design: strategic advances and lessons learned. *Nat Rev* **2007**, 6, 211-219.

Houbraken J, Frisvad JC, Samson RA, Fleming's penicillin producing strain is not *Penicillium chrysogenum* but *P. rubens*. *IMA Fungus* **2011**, 2(1) 87-95.

Huggins J, Zhang ZX, Bray M. Antiviral drug therapy of filovirus infections: S-adenosylhomocysteine hydrolase inhibitors inhibit Ebola virus in vitro and in a lethal mouse model. *J Infect Dis* **1999**, 179 Suppl 1, S240-7.

Huxtable RJ. Biochemistry of Sulfur. University of Arizona Health Sciences Center. Tucson, Arizona. Plenum Press, New York and London. **1986**. Ch. 2.7 & 3.2.

Igarashi K, Kashiwagi K. Modulation of cellular function by polyamines. *Int J Biochem Cell Biol* **2010**, 42 (1), 39-51.

Isaac-Renton JL, Cordeiro C, Sarafis K, Shahriari H. Characterization of *Giardia duodenalis* isolates from a waterborne outbreak. *J Infect Dis* **1993**, 167 (2), 431-40.

Jaganatharaja J, Gowthaman R. Computational screening of inhibitors for HIV-1 integrase using a receptor based pharmacophore model. *Bioinformatics* **2006**, 1 (4), 112-7.

Jarrett JT. The generation of 5'-deoxyadenosyl radicals by adenosylmethionine-dependent radical enzymes. *Curr Opin Chem Biol* **2003**, 7 (2), 174-82.

Jarrett JT. The novel structure and chemistry of iron-sulfur clusters in the adenosylmethionine-dependent radical enzyme biotin synthase. *Arch Biochem Biophys* **2005**, 433 (1), 312-21.

Jorgensen WL. The many roles of computation in drug discovery. *Science* **2004**, 303, 1813-1818.

Karabay O, Tamer A, Gunduz H, Kayas D, Arinc H, Celebi H. Albendazole versus metronidazole treatment of adult giardiasis: An open randomized clinical study. *World J Gastroenterol* **2004**, *10* (8), 1215-7.

Kendrew JC, Bodo G, Dinitzis HM, Parrish RG, Wyckoff H, Phillips DC. A three-dimensional model of the myoglobin molecule obtained by x-ray analysis. *Nature* **1958**, *181* (4610), 662-6.

Kloor D, Oswald H. S-Adenosylhomocysteine hydrolase as a target for intracellular adenosine action. *Trends Pharmacol Sci* **2004**, *25* (6), 294-7.

Knippel R. Effects of MTN enzyme deficiency on *E. coli* O157:H7 Growth and virulence. Master's Thesis, Boise State University May **2013**

Kunze J, Todoroff N, Schneider P, Rodrigues T, Geppert T, Reisen F, Schreuder H, Saas J, Hessler G, Baringhaus KH, Schneider G. Targeting dynamic pockets of HIV-1 protease by structure-based computational screening for allosteric inhibitors. *J Chem Inf Model* **2014**, *54* (3), 987-91.

Kushad MM, Richardson DG, Ferro AJ. 5'-Methylthioadenosine Nucleosidase and 5-Methylthioribose Kinase Activities and Ethylene Production during Tomato Fruit Development and Ripening. *Plant Physiol* **1985**, *79* (2), 525-9.

LeChevallier MW, Norton WD, Lee RG. *Giardia* and *Cryptosporidium spp.* in filtered drinking water supplies. *Appl Environ Microbiol* **1991a**, *57* (9), 2617-21.

LeChevallier MW, Norton WD, Lee RG. Occurrence of *Giardia* and *Cryptosporidium spp.* in surface water supplies. *Appl Environ Microbiol* **1991b**, *57* (9), 2610-6.

Lee JE, Cornell KA, Riscoe MK, Howell PL. Expression, purification, crystallization and preliminary X-ray analysis of *Escherichia coli* 5'-methylthioadenosine/S-adenosylhomocysteine nucleosidase. *Acta Crystallography D Biol Crystallogr* **2001**, *57* (Pt 1), 150-2.

Lee JE, Cornell KA, Riscoe MK, Howell PL. Structure of *Escherichia coli* 5'-methylthioadenosine/S-adenosylhomocysteine nucleosidase inhibitor complexes provide insight into the conformational changes required for substrate binding and catalysis. *J Biol Chem* **2003**, *278* (10), 8761-70.

Lee JE, Settembre EC, Cornell KA, Riscoe MK, Sufrin JR, Ealick SE, Howell PL. Structural comparison of MTA phosphorylase and MTA/AdoHcy nucleosidase explains substrate preferences and identifies regions exploitable for inhibitor design. *Biochemistry* **2004**, *43* (18), 5159-69.

Lee JE, Singh V, Evans GB, Tyler PC, Furneaux RH, Cornell KA, Riscoe MK, Schramm VL, Howell PL. Structural rationale for the affinity of pico- and femtomolar

transition state analogues of *Escherichia coli* 5'-methylthioadenosine/S-adenosylhomocysteine nucleosidase. *J Biol Chem* **2005**, *280* (18), 18274-82.

Lengerich EJ, Addiss DG, Juranek DD. Severe giardiasis in the United States. *Clin Infect Dis* **1994**, *18* (5), 760-3.

Longshaw AI, Adanitsch F, Gutierrez JA, Evans GB, Tyler PC, Schramm VL. Design and synthesis of potent "sulfur-free" transition state analogue inhibitors of 5'-methylthioadenosine nucleosidase and 5'-methylthioadenosine phosphorylase. *J Med Chem* **2010**, *53* (18), 6730-46.

Marr JJ, Müller M. *Biochemistry and Molecular Biology of Parasites*. Academic Press Inc.: San Diego, CA, **1995**. Ch. 3, 5, 6 & 7.

Minotto L, Ko GA, Edwards MR, Bagnara AS. *Trichomonas vaginalis*: expression and characterization of recombinant S-adenosylhomocysteinase. *Exp Parasitol* **1998**, *90* (2), 175-80.

National Toxicology Program. Dept. of Health and Human Services, Metronidazole. *Rep Carcinog* **2011**, *12*, 269-70.

Nillius D, Müller J, Müller N. Nitroreductase (GlnR1) increases susceptibility of *Giardia lamblia* and *Escherichia coli* to nitro drugs. *J Antimicrob Chemother* **2011**, *66* (5), 1029-35.

Nozaki T, Ali V, Tokoro M. Sulfur-containing amino acid metabolism in parasitic protozoa. *Adv Parasitol* **2005**, *60*, 1-99.

Ormond R, Simpkin T, Cornell KA. Cloning and Expression of *Entamoeba histolytica* MTA nucleosidase. Poster Presentation 88th Annual meeting AAAS Boise ID, June **2007**.

Park EY, Choi WS, Oh SI, Kim KN, Shin JS, Song HK. Biochemical and structural characterization of 5'-methylthioadenosine nucleosidases from *Arabidopsis thaliana*. *Biochem Biophys Res Commun* **2009**, *381* (4), 619-24.

Parker NB, Yang X, Hanke J, Mason KA, Schowen RL, Borchardt RT, Yin DH. *Trypanosoma cruzi*: molecular cloning and characterization of the S-adenosylhomocysteine hydrolase. *Exp Parasitol* **2003**, *105* (2), 149-58.

Parveen N, Cornell KA. Methylthioadenosine/S-adenosylhomocysteine nucleosidase, a critical enzyme for bacterial metabolism. *Mol Microbiol* **2011**, *79* (1), 7-20.

Poulin R. *Evolutionary Ecology of Parasites*. Second ed.; Princeton University Press: Princeton, New Jersey, **2007**.

Reguera RM, Redondo CM, Pérez-Pertejo Y, Balaña-Fouce R. S-Adenosylmethionine in protozoan parasites: functions, synthesis and regulation. *Mol Biochem Parasitol* **2007**, *152* (1), 1-10.

Reguera RM, Tekwani BL, Balaña-Fouce R. Polyamine transport in parasites: a potential target for new antiparasitic drug development. *Comp Biochem Physiol C Toxicol Pharmacol* **2005**, *140* (2), 151-64.

Riscoe MK, Ferro AJ, Fitchen JH. Methionine recycling as a target for antiprotozoal drug development. *Parasitology Today*, **1989**, *5*(10) 330-333.

Roberts L, Janovy J Jr. *Foundations of parasitology* 8th Ed. Lincoln Nebraska: Mcgraw Hill Higher Educat **2013**.

Roberts NA, Martin JA, Kinchington D, Broadhurst AV, Craig JC, Duncan IB, Galpin SA, Handa BK, Kay J, Kröhn A. Rational design of peptide-based HIV proteinase inhibitors. *Science* **1990**, *248* (4953), 358-61.

Rzewuski G, Cornell KA, Rooney L, Bürstenbinder K, Wirtz M, Hell R, Sauter M. OsMTN encodes a 5'-methylthioadenosine nucleosidase that is up-regulated during submergence-induced ethylene synthesis in rice (*Oryza sativa* L.). *J Exp Bot.* **2007**, *58*(6), 1505-1514.

Salemme FR, Spurlino J, Bone R. Serendipity meets precision: the integration of structure-based drug design and combinatorial chemistry for efficient drug discovery. *Structure* **1997**, *5* (3), 319-24.

Scallan E, Hoekstra RM, Angulo FJ, Tauxe RV, Widdowson MA, Roy SL, Jones JL, Griffin PM. Foodborne illness acquired in the United States--major pathogens. *Emerg Infect Dis* **2011**, *17* (1), 7-15.

Schramm VL. Enzymatic transition states and transition state analog design. *Annu Rev Biochem* **1998**, *67*, 693-720.

Schramm VL, Gutierrez JA, Cordovano G, Basu I, Guha C, Belbin TJ, Evans GB, Tyler PC, Furneaux RH. Transition state analogues in quorum sensing and SAM recycling. *Nucleic Acids Symp Ser (Oxf)* **2008**, (52), 75-6.

Sharma P, Wollenberg K, Sellers M, Zainabadi K, Galinsky K, Moss E, Nguitragool W, Neafsey D, Desai SA. An epigenetic antimalarial resistance mechanism involving parasite genes linked to nutrient uptake. *J Biol Chem* **2013**, *288* (27), 19429-40.

Simonian MH. Spectrophotometric determination of protein concentration. *Curr Protoc Toxicol* **2004**, *Appendix 3*, A.3G.1-7.

Singh V, Evans GB, Lenz DH, Mason JM, Clinch K, Mee S, Painter GF, Tyler PC, Furneaux RH, Lee JE, Howell PL, Schramm VL. Femtomolar transition state analogue inhibitors of 5'-methylthioadenosine/S-adenosylhomocysteine nucleosidase from *Escherichia coli*. *J Biol Chem* **2005**, 280 (18), 18265-73.

Singh V, Lee JE, Núñez S, Howell PL, Schramm VL. Transition state structure of 5'-methylthioadenosine/S-adenosylhomocysteine nucleosidase from *Escherichia coli* and its similarity to transition state analogues. *Biochemistry* **2005**, 44 (35), 11647-59.

Singh V, Shi W, Evans GB, Tyler PC, Furneaux RH, Almo SC, Schramm VL. Picomolar transition state analogue inhibitors of human 5'-methylthioadenosine phosphorylase and X-ray structure with MT-immucillin-A. *Biochemistry* **2004**, 43 (1), 9-18.

Siu KKW, Lee JE, Sufrin JR, Moffatt BA, McMillan M, Cornell KA, Isom C, Howell PL. Molecular Determinants of Substrate Specificity in Plant 5'-Methylthioadenosine Nucleosidases. *J Mol Biol.* **2008**, 378(1), 112-128.

Sneider W. The discovery of aspirin: a reappraisal. *BMJ* **2000** 321, 1591-1594.

Stanley SL. Amoebiasis. *Lancet* **2003**, 361 (9362), 1025-34.

Stanley SL. Vaccines for amoebiasis: barriers and opportunities. *Parasitology* **2006**, 133 Suppl, S81-6.

Stone B, Eidemiller S, Cornell KA. Characterization of a novel methylthioadenosine nucleosidase (GI885) from *Giardia intestinalis*. Poster presentation Idaho INBRE Conference **2012**.

Tejman-Yarden N, Miyamoto Y, Leitsch D, Santini J, Debnath A, Gut J, McKerrow JH, Reed SL, Eckmann L. A reprofiled drug, Auranofin, is effective against metronidazole-resistant *Giardia lamblia*. *Antimicrob Agents Chemother* **2013**, 57 (5), 2029-35.

Terstappen GC, Reggiani A. *In silico* research in drug discovery. *Trends in Pharmacological Sciences* **2001**, 22(1), 23-26.

Teunis PF, Medema GJ, Schets FM, Havelaar AH. Sedimentation of free and attached *Cryptosporidium* oocysts and *Giardia* cysts in water. *Appl Environ Microbiol* **1998**, 64 (11), 4460-6.

Thome J, When M. Drug Therapy for Common Parasitic Infections within the United States. *US Pharm.* **2012**, 37(8), HS2-HS6.

Thompson RC. Giardiasis as a re-emerging infectious disease and its zoonotic potential. *Int J Parasitol* **2000**, 30(12-13), 1259-67.

Valdez CA, Tripp JC, Miyamoto Y, Kalisiak J, Hruz P, Andersen YS, Brown SE, Kangas K, Arzu LV, Davids BJ, Gillin FD, Upcroft JA, Upcroft P, Fokin VV, Smith DK, Sharpless KB Eckmann L. Synthesis and electrochemistry of 2-ethenyl and 2-ethanyl derivatives of 5-nitroimidazole and antimicrobial activity against *Giardia lamblia*. *J Med Chem* **2009**, 52 (13), 4038-53.

Venkatesan P. Albendazole. *J Antimicrob Chemother* **1998**, 41 (2), 145-7.

Walker J, Barrett J. Parasite sulphur amino acid metabolism. *Int J Parasitol* **1997**, 27 (8), 883-97.

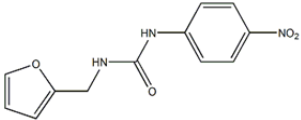
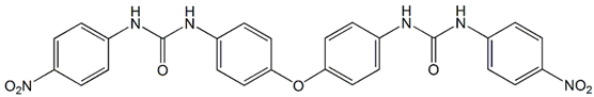
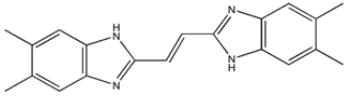
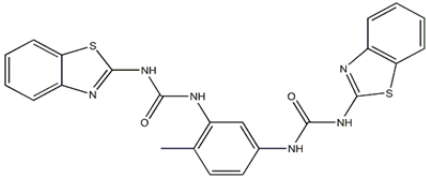
Walsh JA. Problems in recognition and diagnosis of amoebiasis: estimation of the global magnitude of morbidity and mortality. *Rev Infect Dis* **1986**, 8 (2), 228-38.

Zimmer C. *Parasite Rex: Inside the Bizarre World of Nature's Most Dangerous Creatures*. The Free Press: New York, NY, **2000**.

APPENDIX A

Structures and Properties of the Best MTN Inhibitors

Table A.1 Structures and Properties of the Best MTN Inhibitors

Short Name	MW (g/mol)	ϵ ($\mu\text{M}^{-1} \text{cm}^{-1}$) @ λ (nm)	Structure
5A	261.233	0.028 @ 333.4	
8A	528.473	0.050 @ 356.7	
15A	316.4	0.038 @ 371.0	
27A	474.558	0.034 @ 306.0	

APPENDIX B

Substrate Kinetics Graphs

I. *Entamoeba* MTN Substrate Kinetics Graphs

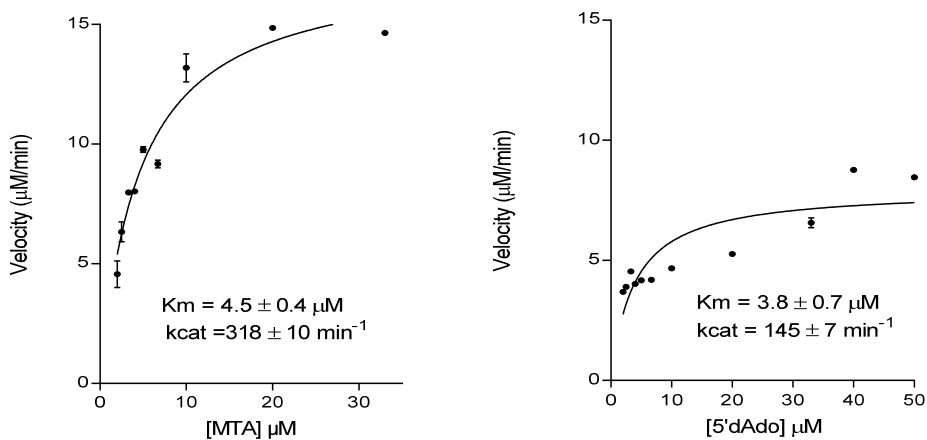


Figure B1. EH MTN Substrate Kinetic Graphs- Left graph is the enzyme velocity with MTA as the substrate and at right is the velocity with 5'dAdo as the substrate.

II. *Giardia* MTN-1 Substrate Kinetics Graphs

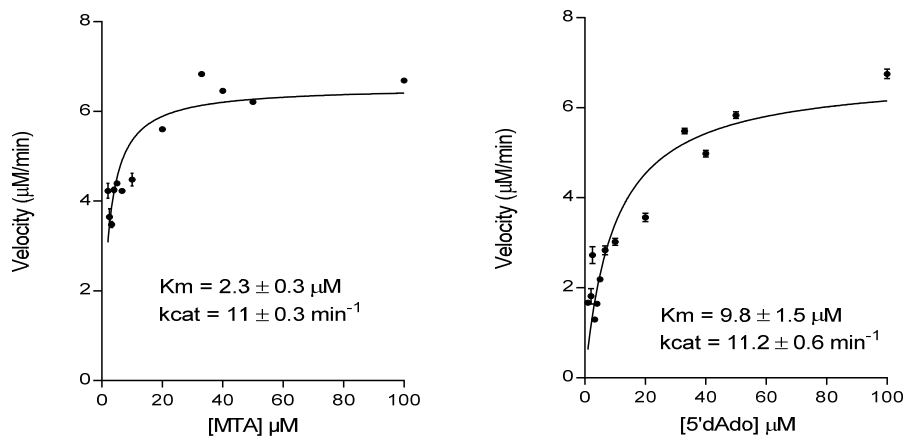


Figure B2. GI MTN-1 Substrate Kinetic graphs – Left graph is the enzyme velocity with MTA as the substrate and at right is the velocity with 5'dAdo as the substrate.

III. *Giardia* MTN-2 Substrate Kinetics Graphs

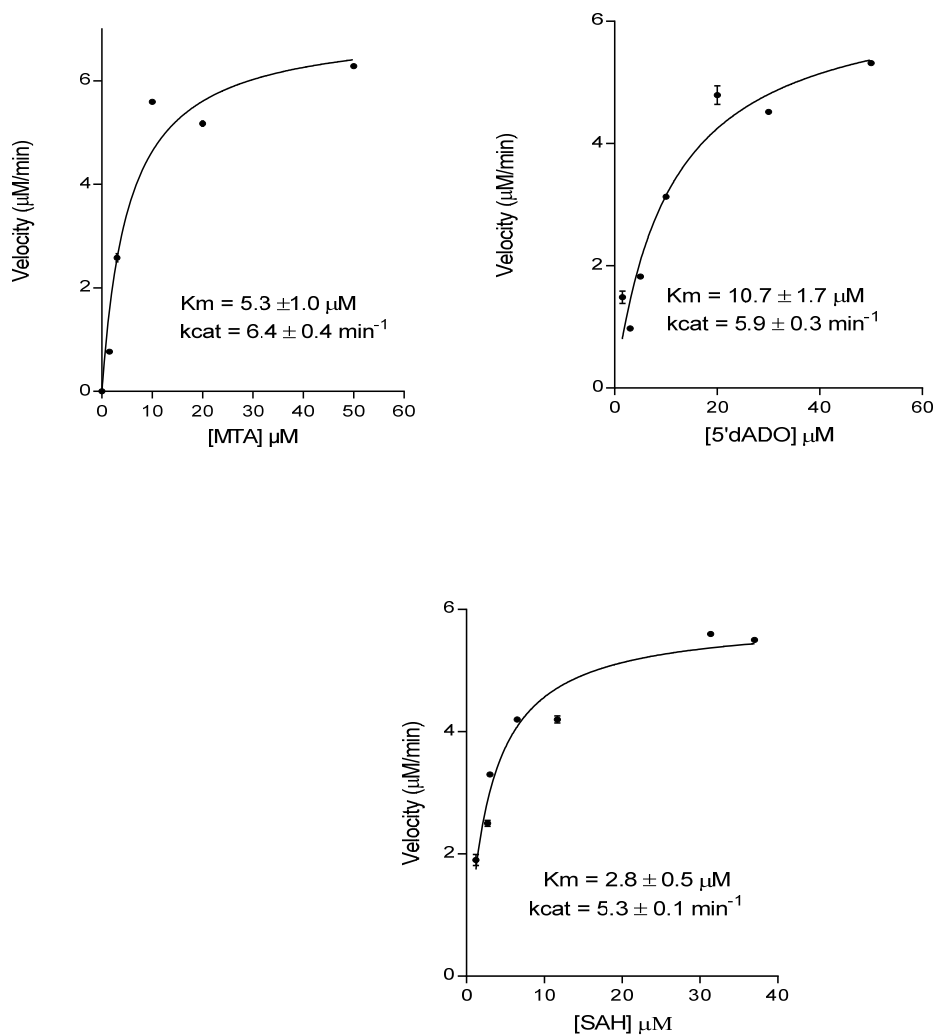


Figure B3. GI MTN-2 Substrate Kinetic Graphs- Top left graph is the enzyme velocity with MTA as the substrate, at top right is the velocity with 5'dAdo as the substrate and at the bottom is the velocity with SAH as the substrate.

APPENDIX C

Graphs of Inhibition Kinetics

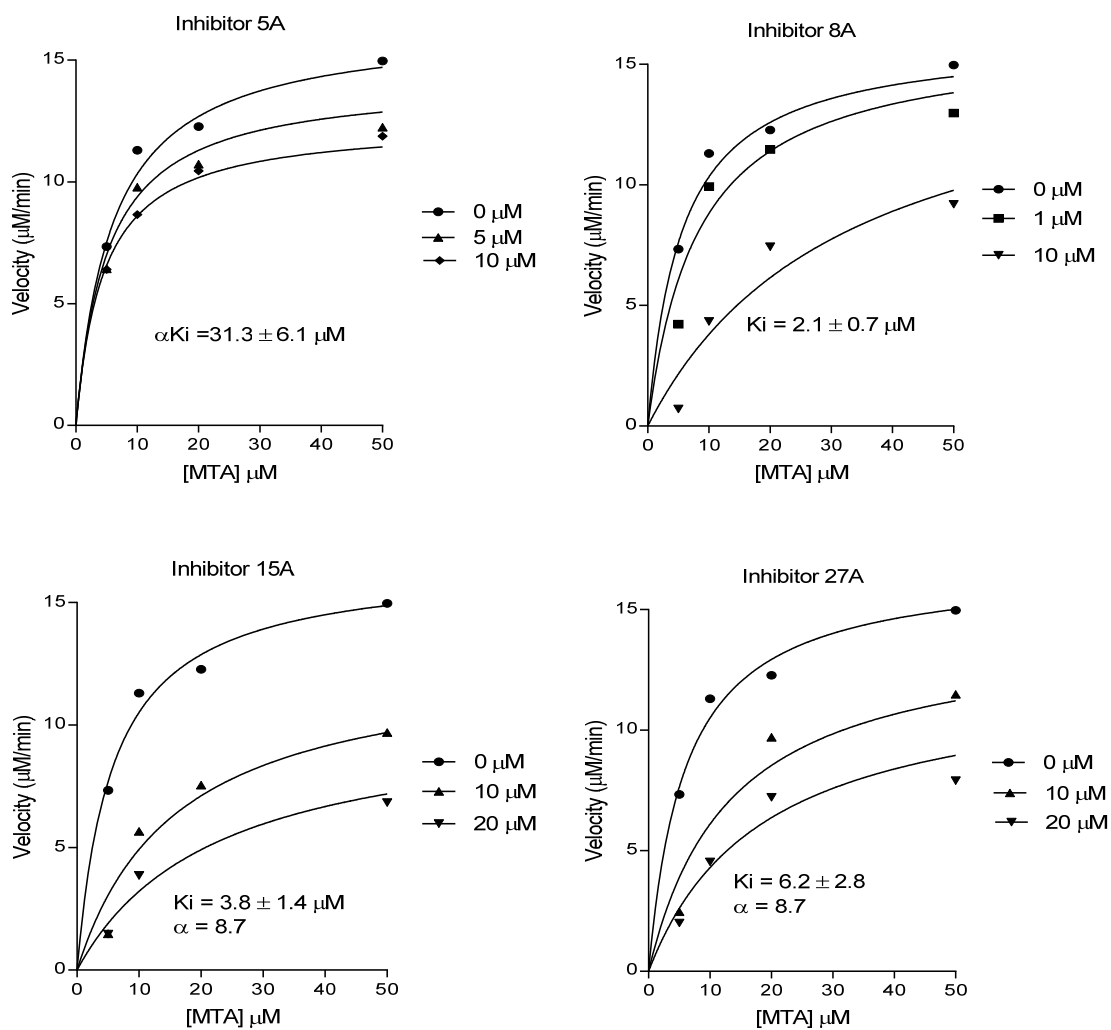
I. *Entamoeba* MTN Inhibition Kinetics graphs

Figure C1. EH MTN Inhibition Kinetics Graphs- Each graph is the substrate v. velocity of EH MTN against inhibitor 5A (top left), 8A (top right), 15A (bottom left), and 27A (bottom right.)

II. *Giardia* MTN-1 Inhibition Kinetics Graphs

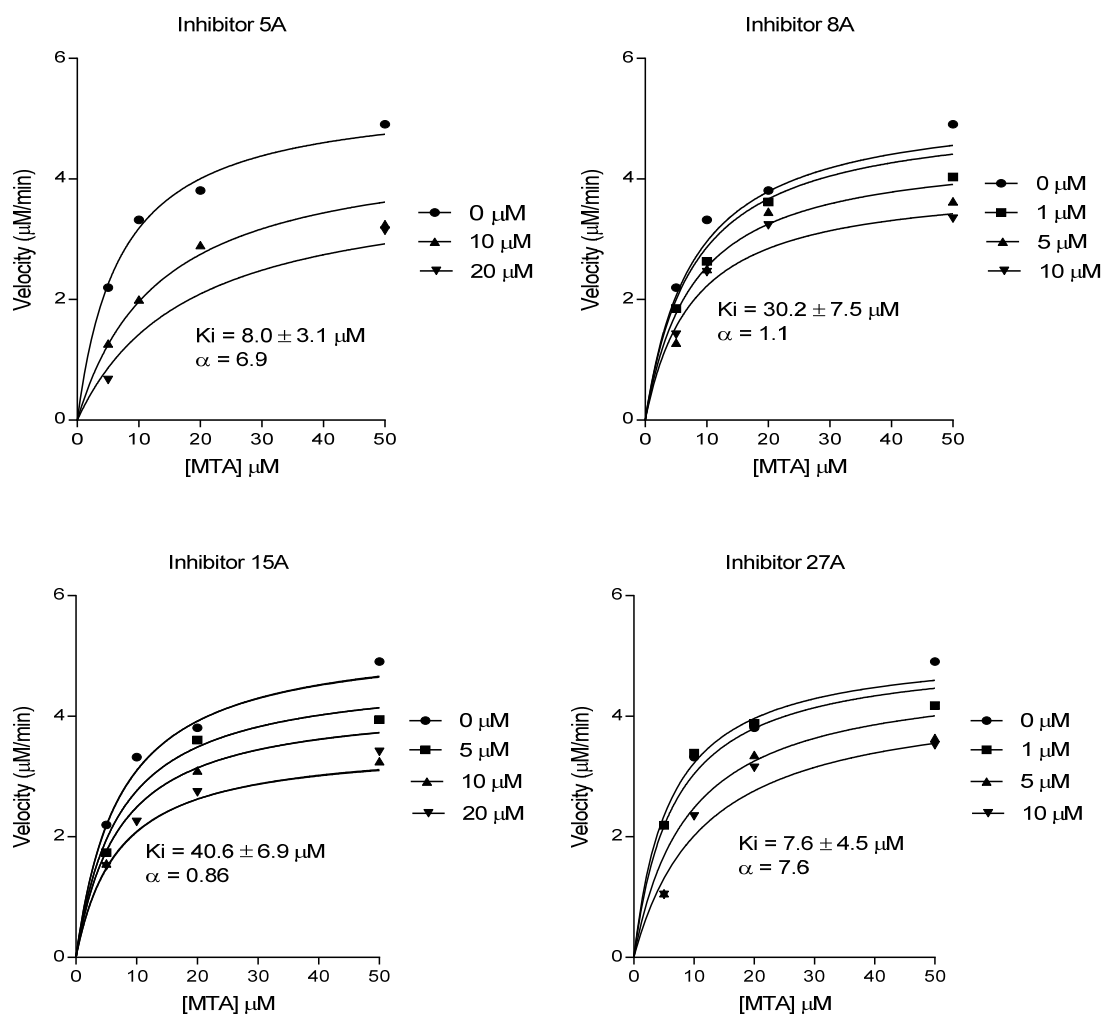


Figure C2. GI MTN-1 Inhibition Kinetics Graphs- Each graph is the substrate v. velocity of GI MTN-1 against inhibitor 5A (top left), 8A (top right), 15A (bottom left), and 27A (bottom right.)

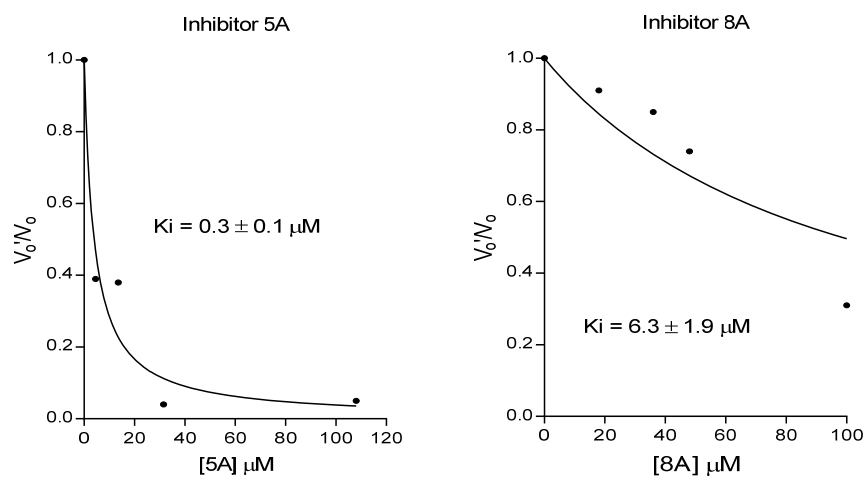
III. *Giardia* MTN-2 Inhibition Kinetics Graphs

Figure C3. GI MTN-2 Inhibition Kinetics Graphs- Each graph shows the enzyme GI MTN-2 being inhibited by drug 5A (left) and 8A (right). These graphs were derived using the method of Singh, Evans et al., 2005.

IV. Human MTA Phosphorylase Inhibition Kinetics Graphs

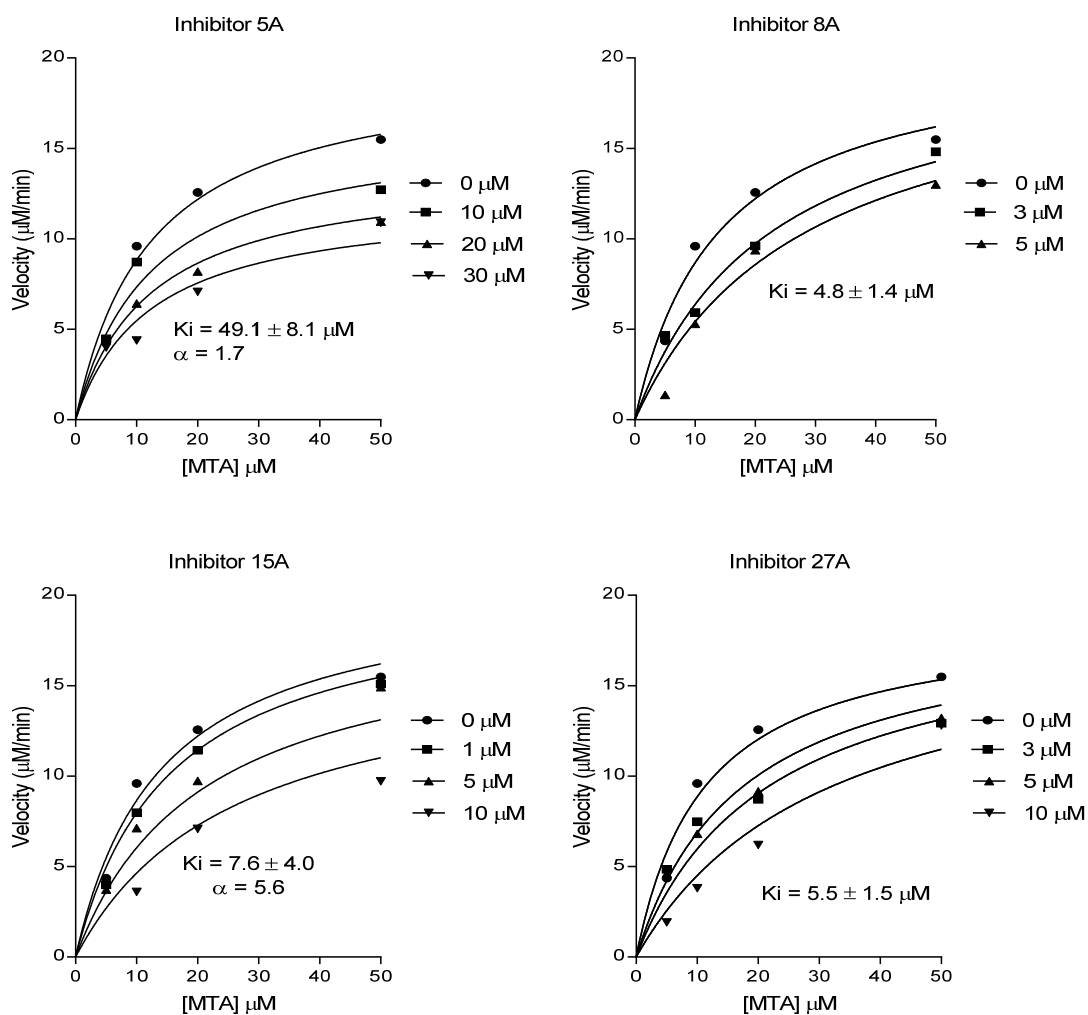


Figure C4. Human MTAP Inhibition Kinetics Graphs- Each graph is the substrate v. velocity of human MTAP against inhibitor 5A (top left), 8A (top right), 15A (bottom left), and 27A (bottom right.)

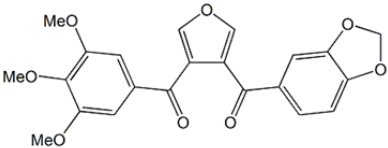
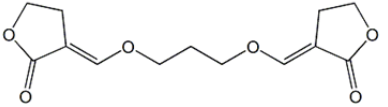
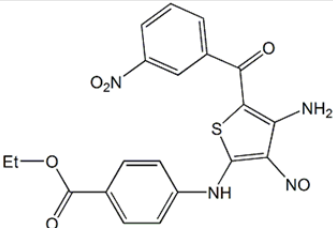
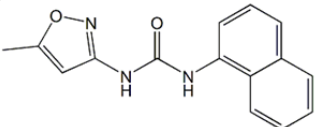
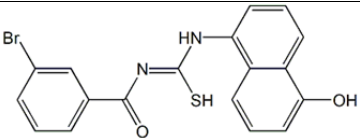
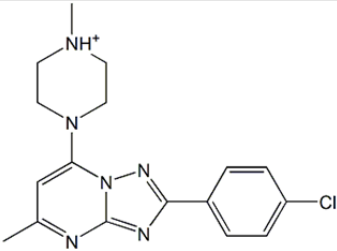
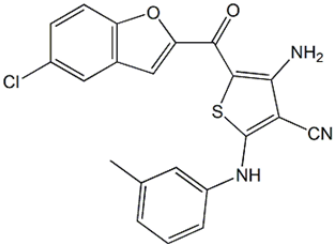
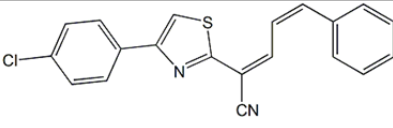
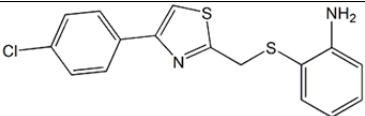
APPENDIX D

Compounds Identified from In Silico Screening

Table D.1 Compounds Identified from *In-Silico* Screening

#	Ligand ID NSC ID CAS # MW	General class	Name	Structure
1	ZINC01163259 4292 5397-96-6	thiazole	1-(2-naphthyl)-2-[(6-nitro-1,3-benzothiazol-2-yl)thio]ethanone	
2	ZINC00035241 35241 6276-41-1 330.39	thiazole	1-(6-nitrobenzothiazol-2-ylthio)-2-phenylethan-1-one	
3	ZINC01668706 36317 No CAS 384.429	piperazine	N,N'-bis(4-methoxyphenyl)piperazine-1,4-dicarboxamide	
4	ZINC01676023 43308 NO CAS 288.3	styrylidine	2-keto-4-phenylimino-N-styrylidene-but-3-enamide	
5	ZINC04776634 45086 NO CAS 261.233	Alkylurea/furan	N-(2-furylmethyl)-N'-(4-nitrophenyl)urea	
6	ZINC18154478 45545 NO CAS 307.284	Pyridine/quinoline	4-[(N'E)-N'-(2,4-dioxo-1H-quinolin-3-ylidene)hydrazino]benzamide	
7	ZINC13154298 55691 7713-86-2 493.238	thiazole	Thiazole, 2,2'-iminobis[4-(4-bromophenyl)-	

8	ZINC04896601 80735 NO CAS 528.473 alkylurea	1-(4-nitrophenyl)-3-[4-[4-(4-nitrophenyl)carbamoylamino]phenoxy]phenyl]-urea	
9	ZINC04900874 87838 NO CAS 346.422 Pyridine/quinoline	1,4-bis(3,4-dihydro-1H-isoquinolin-2-yl)but-2-ene-1,4-dione	
10	ZINC01569416 88600 NO CAS 376.9 piperzine	[4-(2-chlorophenyl)piperazino]-(3,4-dimethoxyphenyl)methanethione	
11	ZINC23118772 91395 NO CAS 396.91 piperzine	1-[4-(3-chlorophenyl)piperazinyl]-3-naphthyloxypropan-2-ol	
12	ZINC29589828 91396 NO CAS 396.91 piperzine	(2R)-1-[4-(2-chlorophenyl)piperazin-1-yl]-3-(1-naphthyloxy)propan-2-ol	
13	ZINC29589833 91397(111210) NO CAS 396.91 piperzine	(2S)-1-[4-(4-chlorophenyl)piperazin-1-yl]-3-(1-naphthyloxy)propan-2-ol	
14	ZINC29589837 91402 NO CAS 376.491 piperzine	(2S)-1-(1-naphthyloxy)-3-[4-(p-tolyl)piperazin-1-yl]propan-2-ol	
15	ZINC04878491 92833 NO CAS 316.4 imidazole	2-[2-(5,6-dimethyl-1H-benzimidazol-2-yl)vinyl]-5,6-dimethyl-1H-benzimidazole	
16	ZINC00111210 111210 NO CAS 348.421 indazole	2-(2-fluorophenyl)-6-phenyl-3-propyl-2H-5,6,7-trihydroindazol-4-one	

17	ZINC01722585 136513 22600-28-8 410.374 furan	DIBENZOYLFURAN DERIV	
18	ZINC05201470 178873 67194-28-9 268.263 furan	3-[3-[(2-oxotetrahydrofuran-3-ylidene)methoxy]propoxymethylene]tetrahydrofuran-2-one	
19	ZINC01735469 201631 NO CAS 436.441 thiophene	4-[[4-amino-3-cyano-5-(3-nitrobenzoyl)-2-thienyl]amino]benzoic acid-ethyl-ester	
20	ZINC00031410 203837 NO CAS 267.283 Alkylurea/ oxazole	N-(5-methyl-3-isoxazolyl)-N'-1-naphthylurea	
21	ZINC05580600 215718 NO CAS 401.277 benzamidine	3-bromo-N-[(5-hydroxy-1-naphthyl)amino-sulfanyl-methylene]-benzamide	
22	ZINC01556940 252359 NO CAS 343.834 Piperazine/ triazole	2-(4-chlorophenyl)-5-methyl-7-(4-methyl-1-piperazinyl)[1,2,4]triazolo[1,5-a]pyrimidine	
23	ZINC01568966 309892 407.873 thiophene	4-amino-5-(5-chlorobenzofuran-2-carbonyl)-2-(m-toluidino)thiophene-3-carbonitrile	
24	ZINC05641037 310347 NO CAS 348.849 thiazole	2-[4-(4-chlorophenyl)-1,3-thiazol-2-yl]-5-phenylpenta-2,4-dienenitrile	
25	ZINC00138096 310365 NO CAS 332.871 thiazole	2-([2-(4-chlorophenyl)-1,3-thiazol-4-yl]methyl)thio)aniline	

26	ZINC01045530 31945 NO CAS 367.422 thiazine	2-(4-hydroxy-3-methoxyphenyl)-4-oxo-6-(3-toluidino)-3,4-dihydro-2H-1,3-thiazine-5-carbonitrile	
27	ZINC01572309 319990 NO CAS 474.558 thiazole	3-(1,3-benzothiazol-2-yl)-1-(5-[[[(1,3-benzothiazol-2-yl)carbamoyl]amino]-2-methylphenyl]urea	
28	ZINC00640726 319994 NO CAS 362.385 Alkylurea/ pyridine	3-(2-methyl-5-[[[(pyridin-3-yl)carbamoyl]amino}phenyl]-1-(pyridin-3-yl)urea	
29	ZINC01574615 329249 NO CAS 348.764 Alkylurea/ thiazole	3-(1,3-benzothiazol-2-yl)-1-(4-chloro-3-nitrophenyl)urea	
30	ZINC05665089 329250 NO CAS 348.764 Alkylurea/ thiazole	1-benzothiazol-2-yl-3-(2-chloro-4-nitrophenyl)-urea	
31	ZINC01574620 329255 NO CAS 329.44 Alkylurea/ thiazole	1-(4-methyl-1,3-benzothiazol-2-yl)-3-[3-(methylthio)phenyl]urea 1-(4-methyl-1,3-benzothiazol-2-yl)-3-[3-(methylthio)phenyl]urea	
32	ZINC01586128 366801 NO CAS 332.828 Alkylurea/pyrazole	N-(1-tert-butyl-3-cyclopropyl-1H-pyrazol-5-yl)-N'-(4-chlorophenyl)urea; nsc366801 N-(1-tert-butyl-3-cyclopropyl-1H...	

33 ZINC00395036 N-[2-methyl-5-(piperidin-1-ylcarbonylamino)phenyl]piperidine-1-carboxamide
375982
20575-74-0
344.451
Alkylurea /
piperdine

